國 立 交 通 大 學

光 電 工 程 學 系 碩 士 班

碩 士 論 文

具高指向性之下埋式金屬光柵光纖波導耦合器

Buried Metal Grating for Vertical Fiber-Waveguide Coupling with High Directionality

研 究 生：吳哲嶢

指導教授：李柏璁 博士

中 華 民 國 一百零一 年 十 月

具高指向性之下埋式金屬光柵光纖波導耦合器

Buried Metal Grating for Vertical Fiber-Waveguide Coupling with High Directionality

研 究 生：吳哲嶢　　Student：Che-Yao Wu

指導教授：李柏璁 博士　　Advisor：Dr. Po-Tsung Lee

國 立 交 通 大 學

光電工程學系碩士班

碩 士 論 文

A Thesis

Submitted to Department of Photonic and Institute of Electro-Optical Engineering

College of Electrical Engineering and Computer Science

National Chiao Tung University

In partial Fulfillment of the Requirements

for the Degree of Master

in

Department of Photonic and Electro-Optical Engineering

October 2012

Hsinchu, Taiwan, Republic of China

中華民國一百零一年十月

具高指向性之下埋式
金屬光柵光纖波導耦合器

研究生：吳哲嶢

指導教授：李柏璁 博士

國立交通大學光電工程系碩士班

摘　　要

在垂直式的光柵耦合器中，耦合效率受到指向性以及光纖模態與繞射光模態的重疊程度所影響。雖然說我們可以利用局部區域的多晶矽的沉積或是在基板與光波導之間加上反射鏡來提升耦合器的指向性，然而這些結構還需要而外的沉積與黃光製程。如果利用金屬來製作我們的光柵結構，我們就可以用較簡易的剝離(lift-off)製程來製作我們的金屬光柵結構。因此在本論文，我們利用金屬光柵並引入了光子晶體之光能隙的概念，將光柵埋至光波導下方，用以降低結構繞射至基板的損耗，因而提升耦合器的指向性。

在模擬當中首先我們探討了，光柵高度、金屬占據比例與氧化層厚度對指向性的影響。從模擬結果中我們可以得知，當光柵的高度為 1000 奈米時，光柵耦合器的指向性能高達 90%。對於一個 200 奈米高的光柵，埋在 1450 奈米厚的二氧化矽裡指向性能達到 80%，此時的耦合效率能達到 65%。而如此高指向性的光柵結構是可以利用較簡易的剝離製程來完成的。緊接著我們又探討了光纖與耦合器的對準對耦合效率的影響，當光纖擺放的角度差兩度時，只會增加 1.19dB 的耦合損耗。而在水平面上的對準上，1 微米的誤差也只會增加 0.32dB 的耦合損耗。

Buried Metal Grating for Vertical Fiber-Waveguide Coupling with High Directionality

Student: Che-Yao wu

Advisor: Dr. Po-Tsung Lee

Department of Photonics and Electro-Optical Engineering Institute, National Chiao Tung University

Abstract (English)

Coupling efficiency of the grating coupler which vertically couples fiber-waveguide is affected by directionality and fiber mode overlap. Although the directionality can be improved by poly-silicon overlay grating structure or additional bottom mirror, these structures need additional fabrication procedures like deposition and lithography. But metal grating structure can be fabricated by easier lift-off process. In this thesis, we design a metal grating which is buried under silicon waveguide, and used the photonic band gap effect of photonic crystal with the grating structure to reduce the substrate loss, and improve the directionality of grating structure.

First, we investigate the dependence of directionality on grating height, filling factor and silicon oxide thickness by simulation. The results show that the grating structure can reach 90% coupling directionality when grating is 1000 nm in height. A metal grating of 200 nm in height, buried in oxide layer of 1450 nm in thickness, can also reach 80% coupling directionality and 65% coupling efficiency. And this high directionality grating structure is adapted to lift-off technique. We also investigate the alignment tolerance of our grating structure. A 2° alignment error in angle results in 1.19dB additional coupling loss. And 1 μm alignment error in lateral only results in 0.32dB additional coupling loss.

Acknowledgements

時光飛逝，碩士的生涯轉眼間就這樣結束了，很慶幸在這碩士的生涯裡能在我的指導教授 李柏璁 博士的指導下學習，您不僅在研究上給予我們指導，讓我有所成長，此外在課餘的時間，老師與我們在排球場上的互動，使我們的生活增添了不少的色彩與歡笑，也讓我從一個完全部會打排球的人，喜歡上排球這項運動。謝謝老師。

再者我要感謝帶領我的林品佐學長，從模擬、製作到實驗量測上的討論與指導，以及最後論文的寫作以及投影片的製作上給予我許多寶貴意見都讓我受益良多。另外要謝謝 贊文、光揚、佳揚與佳裕學長們在研究上提供協助與建議，讓我的研究能更加順利。在鍍膜、蝕刻與黃光的實驗上感謝品睿、為智、權政、開昊、佑政、恆沂的幫忙；也要感謝與我一同進進出出做實驗的宜錩，實驗多在晚上辛苦你了。謝謝已經畢業的學長姐們： 邱立勛、林雋威、呂紹平、許書維、莊文齡在我剛進實驗室時，帶領我熟悉實驗室，熟悉新竹的環境。也感謝在新竹平常陪我打球吃飯的朋友們。因為有你們大家，我在碩士的生活才能過得如此平順精彩，謝謝你們。

特別感謝 交通大學 施閔雄實驗室以及 鄒志偉實驗室在實驗器材上提供的協助，讓此研究能有多方面的嘗試。

最後，我要感謝我的爸爸、媽媽與奶奶在背後默默的關心著我、支持著我讓我能順利的完成碩士這一個階段，也要謝謝我兩位弟弟們的陪伴，讓我的生活精彩。

吳哲嶢 2012 年 10 月 謹誌於 新竹交通大學 交映樓

Table of Contents

Table Captions

Chapter 2

Chapter 4

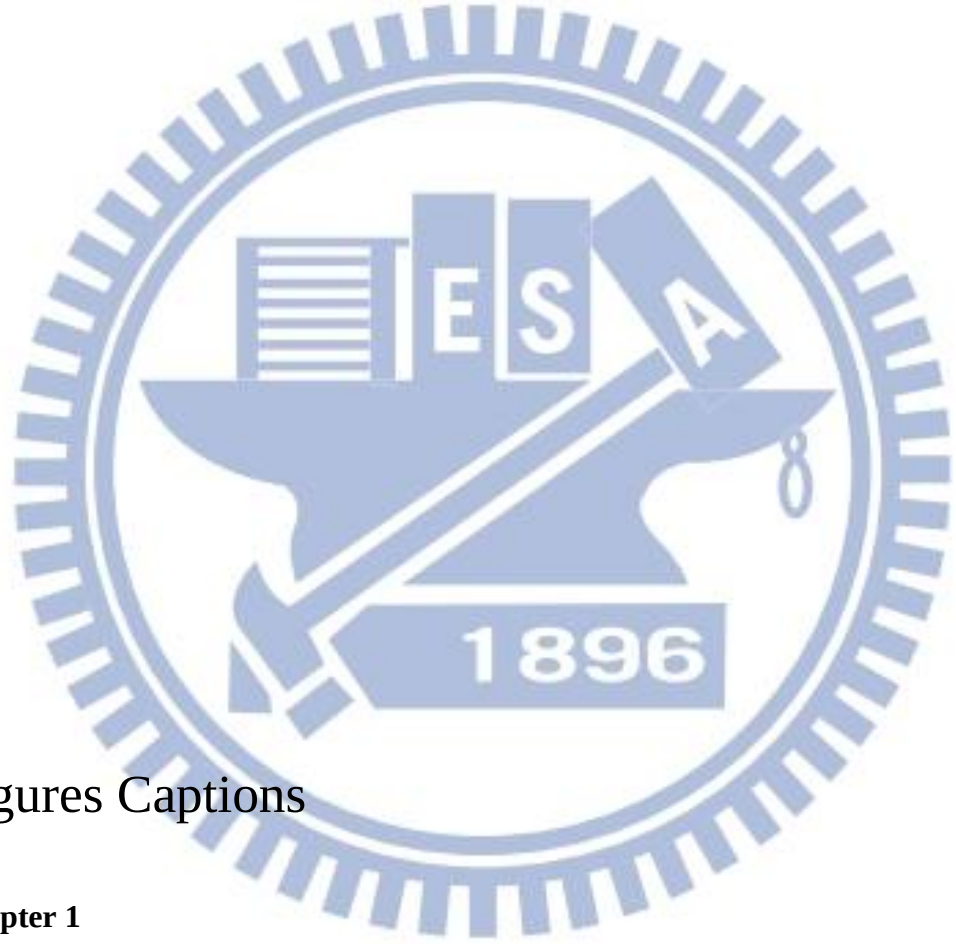

Figures Captions

Chapter 1

Chapter 2

Chapter 3

Chapter 4

Chapter 1.

Introduction

1-1. Coupling into optical integrated circuits

Photonic integrated circuits made on silicon-on-insulator (SOI) platform with high refractive index contrast can confine light in sub-wavelength extends. It greatly reduces footprint of photonic devices, and is compatible with standard fabrication processes for complementary metal-oxide semiconductor (CMOS) [1]. However, an inevitable trade-off accompanies miniaturizing device size is the large mode mismatch in size and shape between photonic waveguides and single mode fibers. Therefore it will becomes more and more challenging to couple light into such small photonic circuits.

1-1-1. Butt-coupling

The most intuitive way to couple light into optical waveguide is from one of its end which is called butt-coupling. Many researchers had studied for coupling light from fiber into optical waveguide in this scheme. Because the core cross-section of typical optical fibers (of about 8 μm diameter) are much larger than that of photonic waveguides, butt-coupling with mode size converter is one solution to improve efficiency[2-8]. In 2002 Morita *et al.* designed inverse taper to serve as mode size converter between the silicon wire and the silicon-based waveguide [3]. As Fig. 1-1 shows, the inverse tapper was embedded inside a high-index polymer waveguide with

3 μm × 3 μm cross-section. The structure is optically equivalent to a silica-based waveguide, and the taper was connected directly to the silicon-wire waveguide. The cross-section of the silicon-wire waveguide was 0.3 μm × 0.3 μm to achieve a single mode condition. The very low mode size conversion loss 0.8 dB (83.2% coupling efficiency) is obtained when the taper tip width less than 60 nm and taper is 200 μm long. In 2003 Manolatou *et al.* developed a three-dimensional adiabatic-taper [5]. As shown in Fig. 1-2, optical fiber can be simply butt coupled to the large end of the taper. Then the 3D taper couples the fiber mode into a 240 nm silicon channel waveguide implemented in SOI platform. With this design they can couple light from single mode fiber with circular mode of about 10 μm diameter to sub-micrometer silicon channel waveguides of 250 nm × 250 nm cross-section. Their simulation showed that nearly all the power is efficiently compressed to 240 nm mode size. They also did the experiment by coupling light from a fiber to a 10 μm three-dimensional mode converter where it tapers down to a 240 nm slab mode. And the optical coupling losses were very high at 16-17 dB (2-2.5% coupling efficiency).

Although butt-coupling can achieve good coupling efficiency by using these inverse taper structures, it requires wafer-cleaving which is undesirable for chip system and will make photonic circuit design difficult. Besides, it needs precise alignment between fiber and waveguide, which will lift the operation criterion. Fortunately, these difficulties can be avoided by using grating structures to couple light from vertically arranged fiber into on-chip waveguides.

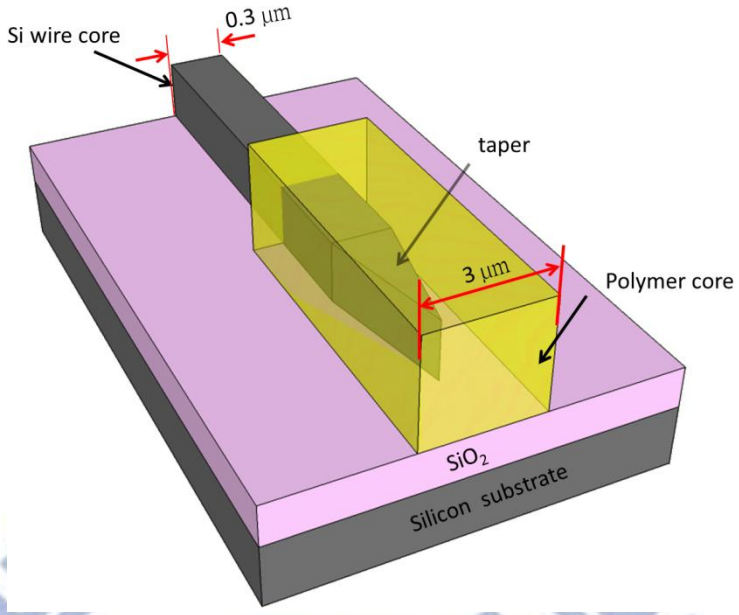

Fig. 1-1. Schematic diagram of proposed mode size converter for silicon wire.

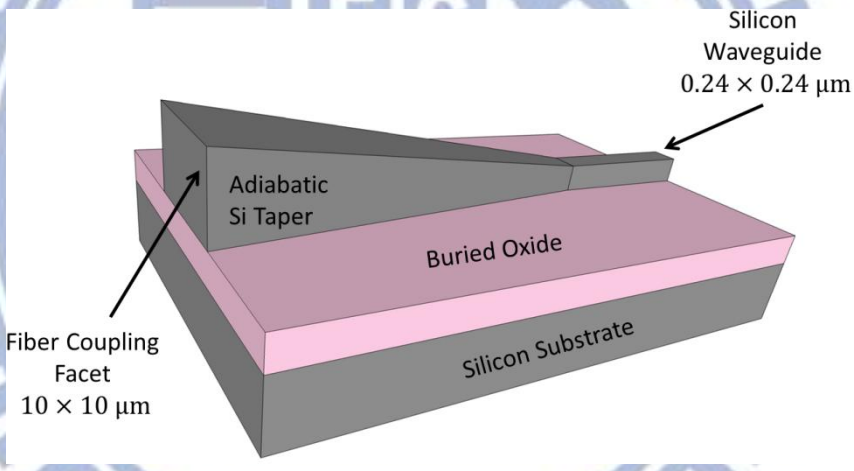

Fig. 1-2. Schematic view of an adiabatically tapered 3D silicon mode converter implemented in SOI technology.

1-1-2. Out of plane coupling

Grating structure can be utilized to couple light in and out of optical waveguides with fibers nearly perpendicular to chip surface. This technique will raise freedoms of photonic circuit design and enable wafer-scale testing because there is no need to cleave the chip. In order to efficiently coupling light between photonic waveguide and single mode fiber, there are two important factors we need to consider; one is mode

match between the field profiles of diffracted light from grating and fiber mode. The problem of mode mismatch can be solved by using apodized grating structure, which can diffract waves in Gaussian-like profile for matching fiber mode and has been proposed [9, 10]. Another important factor is directionality defined as the percentage of light power that propagates along waveguide and is finally diffracted upward toward coupling fiber. Without any design, grating will diffract waves propagating in waveguide, and the diffracted waves will transmit upward and downward with equal power. Therefore the directionality is naturally limited to 50 %. For directionality beyond 50 %, many designs had been proposed [11-19]. In 2006, Laere et al. added a gold bottom mirror to the structure which can reflect downward diffraction back to upward counterpart and improve the directionality [12]. As shown in Fig. 1-3, the grating structure and waveguide is first covered by BenzoCycloButene (BCB). Then gold mirror is evaporated on it. Finally the whole structure is bonded with another BCB-layer onto a host-substrate and grating coupler with gold bottom mirror is completed. The theoretical coupling efficiency to nearly vertical arranged fiber is 72%. Another scheme for improving directionality is achieved by increasing vertical asymmetry in the grating structure. In 2006 Roelkens et al. presented a grating structure made on locally deposited poly-Silicon overlay on optical waveguide as depicted in Fig. 1-4. The grating structure is etched through the overlay and shallow-etched to the waveguide. The overlay changes diffraction property of the grating which will provide batter directionality and improve coupling efficiency to 66 % when coupling fiber is 10 degrees with respect to vertical axis [13].

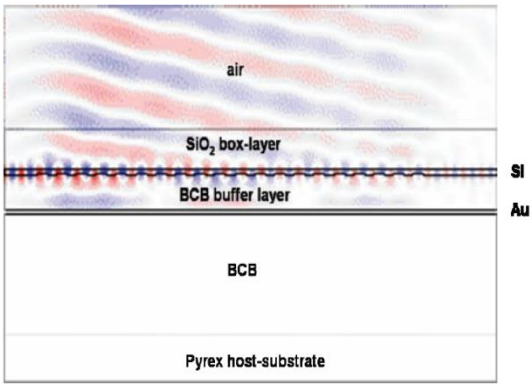

Fig. 1-3. The cross-section of the fabricated structure.

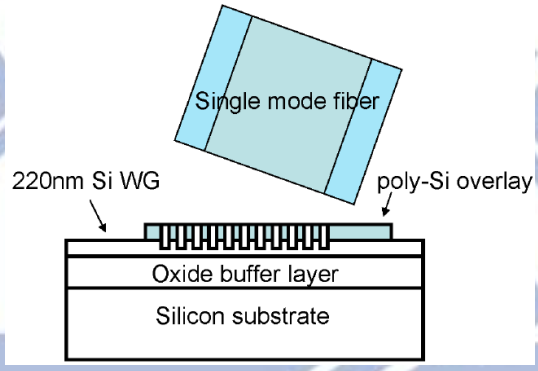

Fig. 1-4. Schematic illustrating the grating structure with poly-silicon overlay.

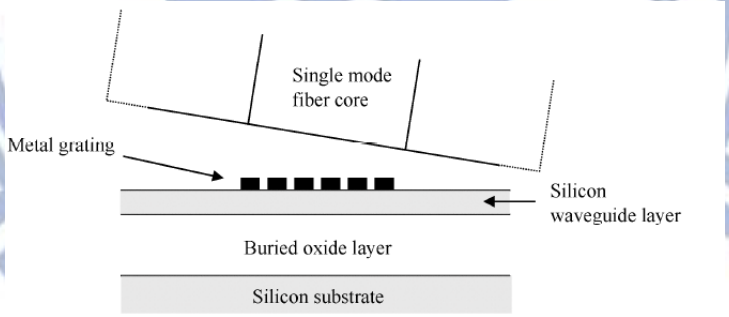

Fig. 1-5. Metal grating on top of an SOI-waveguide for coupling to a single mode optical fiber.

However for improving directionality, there are always structures, except grating itself, requiring additional fabrication procedures like deposition and lithography. That will complicate the fabrication and raise the cost. So we aim at designing a simple structure which can provide certain vertical asymmetry and generate high directionality. In 2007, Scheerlinck et al. had used simple lift-off technique to make metal grating on waveguides [20]. The metal grating coupler layout is depicted in Fig.

1-5. At a wavelength of 1550 nm, there is a very high refractive index contrast between the metal stripes and the surroundings. Thus, light incident on the grating is strongly scattered. Although metal is introduced, loss does not dominate because it is not bulk and only occupies a small portion. Only few periods is needed for obtaining comparable coupling efficiency due to the strong scattering. In this scheme the utilization of lift-off technique for producing metal grating is most attractive because of its simplicity.

1-2. One dimensional Photonic Crystal for metal grating

Grating structure with periodically distributed materials should provide some artificial dispersion relations other than additional wave vectors. However to our knowledge only the diffraction phenomenon has been utilized. If we can utilize its artificial dispersion relation, we may be able to generate a vertically asymmetric structure to improve directionality. This is the target of our work.

In solid state physics, scientists discovered the periodic variation of atomic potential in crystal determines the energy band structure and conduction behavior of electrons. In 1987, Eli Yablonvitch [21] and Sajeev John [22] first proposed the concept of photonic crystal, a periodic environment for photons that can provide interesting characteristics similar to that of electrons behave in solid state crystal, for example the photonic band structure and photonic band gap, which relate to energy band structure and energy band gap.

One of the simplest possible photonic crystals is multilayer film. As shown in Fig. 1-6 the structure is periodic in z direction and homogeneous in xy plane. Propagation of light in photonic crystal can be affected significantly by diffraction

coupling between optical modes, result in interesting dispersion characteristics which forms photonic band diagram. By changing the lattice geometry or contrast of dielectric constants, there will open specific frequency ranges, named photonic band gap (PBG), can completely forbid propagation of electromagnetic wave in z direction through the one-dimensional photonic crystal. Fig. 1-7 shows the band diagram of the multilayer structure formed by alternating gold and air layers. And the communication wavelength 1550 nm is just within the band gap when grating period is 610 nm. Therefore 1550 nm waves with z direction component will propagate evanescently in this periodic structure. Constructing this grating on one side of the waveguide will generate the vertical asymmetry we want.

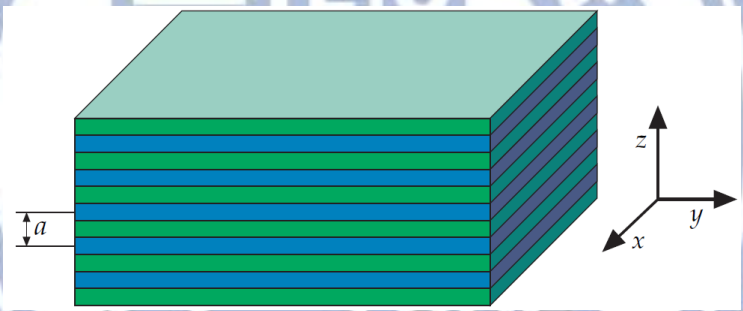

Fig. 1-6. The one-dimensional photonic crystal.

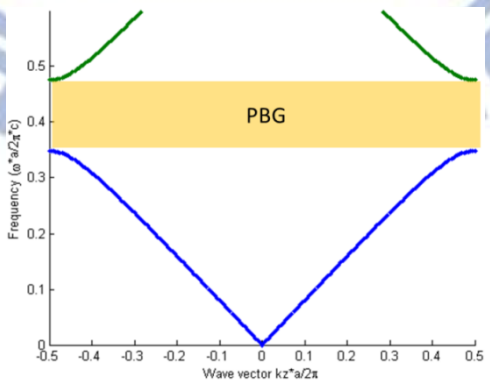

Fig. 1-7. The band diagram of the grating structure with period of 610 nm.

1-3. Motivation

In order to efficiently couple light into integrated photonic circuits without wafer-cleaving, grating structures shows their ability to couple light from vertically arranged fiber into on-chip waveguides. In earlier designs, although the grating structure with poly-silicon overlay or additional metal bottom mirror can generate high directionality, those structures always need additional fabrication processes. Metal grating coupler not only simplifies fabrication processes by lift-off technique, its high index contrast with respect to surrounding also make the diffraction only need few periods. Thus the coupler footprint can be small. Besides, grating structure can be considered as one-dimensional photonic crystal. When operating wavelength is in band gap of the grating structure, waves propagating through will be forbidden. Only diffracted waves propagating toward the coupling fiber is allowed. Therefore coupling between on chip waveguides and vertical arranged fibers will be more efficient with higher directionality. For doing this we design a metal grating which is buried in oxide layer under the silicon waveguide. This grating structure can forbid diffractions toward substrate by grating itself, so it can have high directionality without need of any additional structure.

Chapter 2.

Theoretical characterization and structure design

2-1 Phase matching condition

When waveguide mode propagating (in z direction) with propagation constant β impinges on the grating structure, it will be provided an additional wave vector by the grating as illustrated in Fig. 2-1. The additional wave vector is m times of reciprocal lattice $K = 2\pi/a$ of the grating, where m is an arbitrary integer and a is the grating period. The hybrid propagation constant can be expressed as $\beta - mK$ (denoted by vertical dash lines). When it matches z-component of radiation wave vector $2\pi/\lambda$ (crossing with dotted circle), the waveguide mode will be diffracted out. The z-component of the diffracted wave can be expressed as

$$k_{z,m} = \beta - mK, \tag{2-1}$$

where m is the integer denoting diffraction order and subscription z indicates

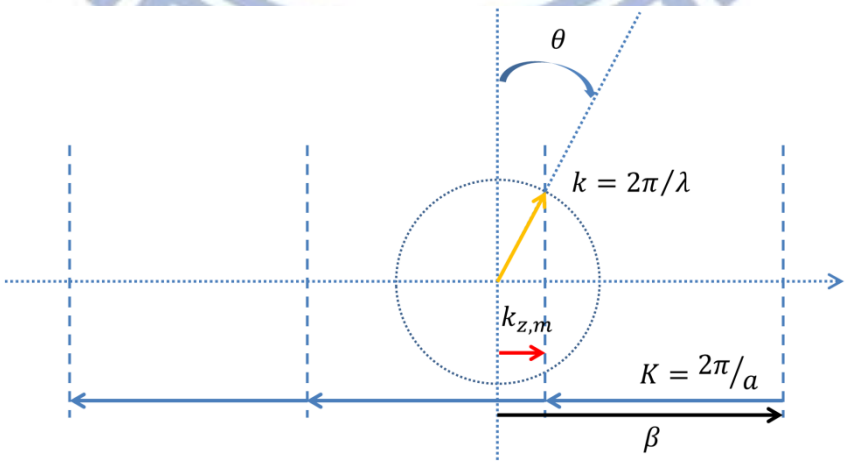

Fig. 2-1. Phase matching conduction graphically illustrates the occurrence of different diffraction orders.

z-component. Finally the diffraction angle θ is determined by λ, β and K. Note that waves will be diffracted upward toward coupling fiber and downward toward substrate simultaneously.

By properly design the grating structure, diffraction can be limited to a single diffraction order (only one vertical dash line crosses the dotted circle). And it allows efficient coupling between the optical fiber and the photonic integrate circuit. In our grating structure the grating period of 610 nm is chosen for yielding diffraction of single order with single diffraction angle ($\theta \sim 8°$) around 1550 nm. The nonzero diffraction angle is intended because a zero diffraction angle occurring in the case of $\beta = K$ will accompany severe back-reflection into the waveguide.

2-2 Finite element method

For numerical investigation we simulate waves propagating along waveguide and diffracted by grating by using finite element method (FEM). The method is provided by Comsol software and is a numerical technique for solving problems of physics consisted of partial differential equations (PDE) with a series of well-defined boundary conditions. The problems can be solved independent of time evolution. So its advantage is time-saving. For complicated optical systems, it can solve boundary value problem, eigenvalue problem and find steady state solution of a system by employing variational method. To apply this method, it requires discretizing a continuous domain into a set of discrete sub-domains, usually called elements, and the solution of each element would be approximated by certain characteristic form to solve the problems.

Here, the wave equations in the frequency domain for the magnetic and the electric fields are

$$\nabla \times \left(\varepsilon^{-1}(\vec{r})\nabla \times \vec{H}(\vec{r})\right) = \frac{\omega^2}{c^2}\vec{H}(\vec{r}) \tag{2-2}$$

$$\varepsilon^{-1}(\vec{r})\nabla \times \nabla \times \vec{E}(\vec{r}) = \frac{\omega^2}{c^2}\vec{E}(\vec{r}) \tag{2-3}$$

where c is the speed of light in vacuum. To solve the wave equation for either magnetic or the electric field in frequency domain together with boundary conditions, standard FEM method proceeds in three steps [23]. First, the wave equations are identified as solutions of certain variational problems where boundary conditions at the surface ∂V have been incorporated as additional terms of lagrangian L. The most general variational formulation for the electric field is given by

$$L(\vec{E}) = \int_V dr^3 \left[\frac{1}{\mu}(\nabla \times \vec{E}) \cdot (\nabla \times \vec{E}) - \frac{\omega^2}{c^2}\varepsilon\vec{E} \cdot \vec{E}\right] + \int_{\partial V} d\vec{S}[\frac{\gamma_e}{2}(\vec{\mathrm{n}} \times \vec{E}) \cdot (\vec{\mathrm{n}} \times \vec{E}) - \vec{E} \cdot \vec{U}] + i\frac{\omega}{c}\sqrt{\frac{\mu_0}{\varepsilon_0}}\int_V dr^3\vec{E} \cdot \vec{j} \tag{2-4}$$

where μ is the magnetic permeability and ε is dielectric function both may varied in space. In addition, $\vec{n}$ denotes the outward normal at the surface ∂V and the electric field has to satisfy the Dirichlet boundary condition $\vec{n} \times \vec{E} = 0$ on ∂S. γ_e and $\vec{U}$ are known quantities which are used represent various other types of boundary conditions such as impedance boundary conditions and Sommerfeld radiation conditions. Finally, radiation sources within the computational domain V are described through the spatially varying current density $\vec{j}$.

The second step is the most demanding step which consists of the discretization of the Lagrangian. The computational domain V is divided into a number of

small-volume elements, the so-called finite elements. Within each element, the electric field is expanded into a series of certain elementary functions with unknown coefficients. It becomes possible to approximately enforce the div-conditions of the electric field within a given element as long as the dielectric function does not vary within this element. Fig. 2-2 show the model with/without mesh generation in someone case.

In the final step, these expansions facilitate the transformation of the variational eqs. 2-4 into a sparse set of linear expansions via the Galerkin method. This matrix system can subsequently be solved via advanced linear algebra methods, either for obtaining eigenfrequencies and eigenmodes of the system of interest or to determine scattering cross sections of complex structures as well as transmittance and reflectance through functional elements.

An additional advantage of using FEM of COMSOL is its nun-uniform mesh rule which fits especially for critical structures. Besides, the mesh of each part can be defined individually depending on its importance. So we can largely save computer memories for calculation, and get the simulation results quickly. Finally its capability in post processing is almost impeccable. We can get all information we need, such as transmittance, reflectance, and field distributions, from a single simulation.

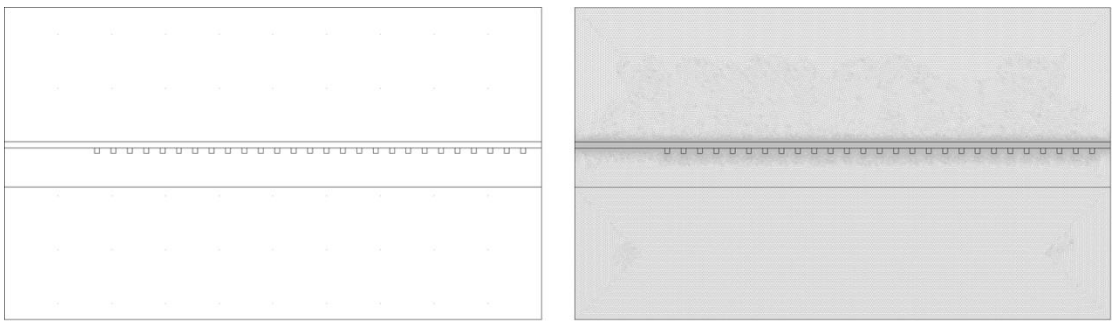

Fig. 2-2. The model (a) before (b) after mesh generation.

2-3 Plane-Wave-Expansion method

Because we intend to take advantage of periodicity of the grating structure, we have to understand the effect caused by periodicity. PWE method is an efficient and useful way to obtain the dispersion relation of a given periodic structure. According to the Bloch theorem, eigen-function in a periodic system can be expressed as the product of periodic envelope and plane-wave function. The main idea of *PWE* simulation is expressing the dielectric function and periodic function in Bloch function as Fourier expansion:

$$\varepsilon^{-1}(\vec{r}) = \sum_{\vec{G}} \varepsilon_{\vec{G}}^{-1} e^{i\vec{G}\cdot\vec{r}} \qquad (2\text{-}5)$$

$$\vec{H}(\vec{r}) = \sum_{\vec{G}} \vec{h}_{\vec{k}}(\vec{G}) e^{i(\vec{k}+\vec{G})\vec{r}} \qquad (2\text{-}6)$$

where vector $\vec{G}$ is reciprocal lattice vector. The Fourier coefficient can be expressed as $\varepsilon_{\vec{G}} = \frac{1}{V_c}\int_{unit\ cell} \varepsilon(\vec{r}) e^{-i\vec{G}\cdot\vec{r}}$, where V_c is the volume of the unit cell. By substituting equations (2-5) and (2-6) into master equation, the master equation becomes

$$(\vec{k}+\vec{G})\sum_{\vec{G'}} \varepsilon_{\vec{G}-\vec{G'}}^{-1}(\vec{K}+\vec{G'}) h_{\vec{k}}(\vec{G'}) = -(\frac{\omega^2}{{c_0}^2}) h_{\vec{k}}(\vec{G'}) \qquad (2\text{-}7)$$

With different in-plane *k*-values along the *1st* Brillouin zone, which is determined by the *PhC* structure, several $\vec{G}$ vectors are used to obtain numerous coupled equations. In the computation, proper and finite numbers of plane-waves (linear combinations of $\vec{G}$ vectors) are used to increase accuracy of the solved dispersion relation. In these coupled equations, we can obtain the eigen-values $(\frac{\omega^2}{{c_0}^2})$ and dispersion relation

($\frac{\omega}{c}$ $v.s.\boldsymbol{k}_{//}$) by matrix diagonalization method. Finally we will know whether the operating wavelength is in photonic band gap or not and design the structure we need.

2-4 Simulation results

Fig. 2-3 (a) illustrates the model and computational domain used in this study. The grating structure is made of gold strips (refractive index n = 0.55+11.5i @ 1550 nm) separated by period a of 610 nm, and is buried in the oxide layer (n = 1.45 with thickness d) under 220 nm silicon waveguide (n = 3.46). In order to avoid reflections at the interface between fiber and air, index matching glue (n = 1.45) is introduced between the optical fiber and the waveguide. Light propagating in the waveguide will finally be diffracted by the grating structure. Some portion will be diffracted upward directly toward the fiber (denoted as ray a). The other portion will be diffracted downward and reflected by the substrate interface (denoted by ray b). Therefore the thickness of oxide layer will affect the interference between rays a and b. This will be discussed in the following sections. For comparison we also construct upright gold grating (Fig. 2-3 (b)) as reference with stripes standing on the waveguide instead of buried under it.

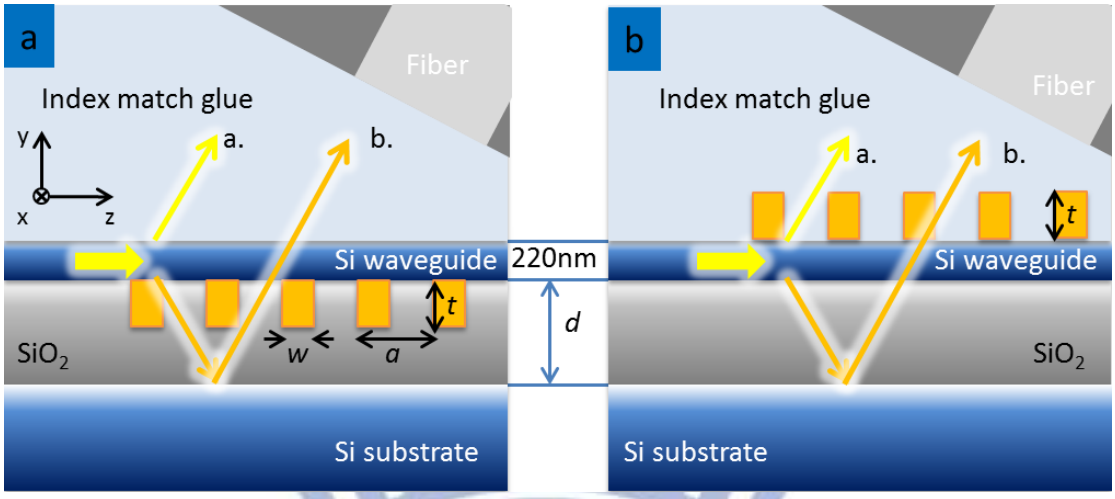

Fig. 2-3. Schematic illustration of (a) the proposed buried grating coupler and (b) the upright grating coupler.

There are many parameters which will affect the directionality, such as grating high *t*, oxide thickness *d*, and filling factor (grating width, *w*, to period ratio, *w*/*a*). Here we set negative *t* values as buried gratings and positive *t* values as upright gratings. To know the character as well as the maximum directionality of our grating design, we used the commercial software COMSOL to carry out the detailed two-dimensional finite element numerical analysis. The material properties of waveguide, glass substrate, and surrounding index matching glue were taken into consideration while solving for the electromagnetic field distribution.

In this work, wave propagating along the waveguide is at wavelength of 1.55 μm and is transverse-electric (TE) polarized fundamental mode. The waveguide mode is calculated by package of boundary mode analysis in the software. Because the wave is TE polarized without components perpendicular to metal-dielectric interface, no surface plasma resonance would be induced at the metal grating region.

2-4-1 Dependence of directionality on grating height

We first fix filling factor (FF) $\frac{w}{a}$ to be 30% as suggested in [20], and investigate the dependences of directionality on *t* when oxide thickness $d = 1.35$, as illustrated in Fig. 2-4 (a). At first we consider the case of upright grating. The directionality reaches a peak value about 64% at $t = 40\,\text{nm}$. For smaller *t*, the directionality decreases to zero due to the reduction in grating strength. In this situation, most energy would transmit though the grating region without being diffracted. On the other side, the grating with larger *t* can be regarded as a one-dimensional photonic crystal with gold and index-matching glue distributed periodically in z direction. Band diagram of the one dimensional photonic crystal with period *a* = 610 nm and FF = 30% is shown in Fig. 2-4 (b). The wavelength of 1.55 μm is just within the photonic band gap (PBG) and therefore waves will propagate evanescently. Thus less diffracted wave would be able to transmit through the grating of larger *t*, and the directionality decreases exponentially. Next we consider the case of buried grating coupler. For *t* ranging from 0 to -40 nm, the directionality of the buried grating coupler is similar to that of the upright grating with *t* from 0 to 40 nm. And when *t* becomes more negative, the grating structure can again be regarded as a one–dimensional photonic crystal. However in this case, the grating is buried under the waveguide. PBG effect would forbid diffracted waves of 1.55 μm propagating downward. More of the diffraction would propagate upward toward fiber and thus the directionality increases progressively and finally saturate as high as 90%. The remaining 10 % is caused by inevitable absorption of metal. Before it saturates, the directionality oscillates as a function of *t*. This is resulted from the interference between waves diffracted upward and reflected from the substrate interface (denoted by rays a and b in Fig. 2-3 (a) respectively). We will discuss this feature in the following section.

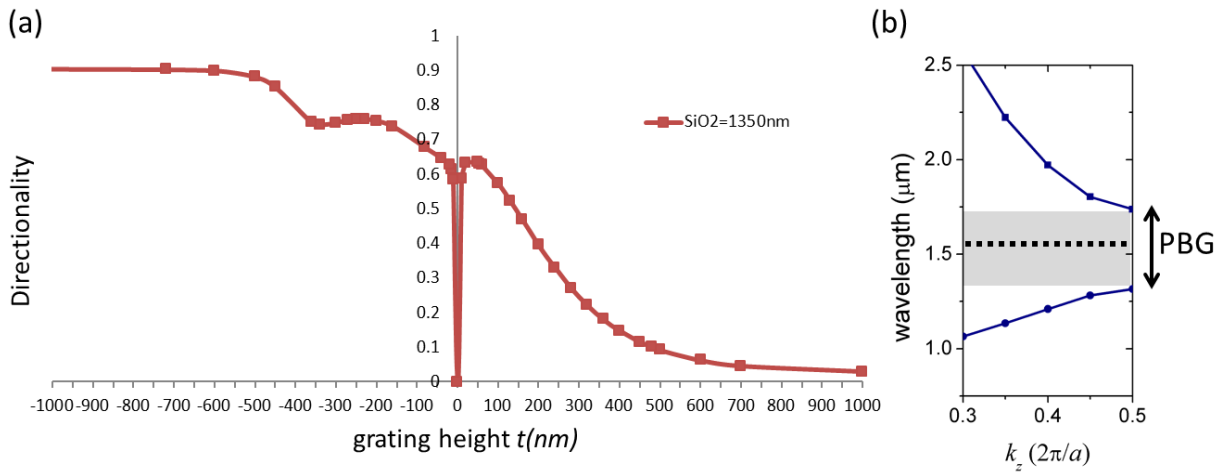

Fig. 2-4. (a) The relations between directionality and grating height under two different thicknesses of oxide layer. (b) The band diagram of grating infant grating structure with FF = 30%.

2-4-2 Dependence of directionality on the thickness of oxide layer

In this part we investigate the dependence of directionality on thickness *d*. For upright grating, 40 nm grating height for example, the directionality oscillates with *d* as shown in Fig. 2-5 (a). This is because the optical path length (OPL) of ray b in Fig. 2-3 (b) first propagating downward and being reflected by the substrate depends on *d*. The reflected component interferes with ray a and causes the directionality oscillation. The interference also occurs in the buried case. Thus the relations of directionality and oxide thickness are similar for buried grating, as shown in Fig. 2-5 (b). For practical consideration, it is much difficult to fabricate buried metal grating with more negative grating height. Here we investigate -200 nm buried grating as a target. From the dependence of directionality on oxide thickness, we find that the maximum directionality for -200 nm buried grating happens when d = 1.45 μm instead of 1.35 μm.

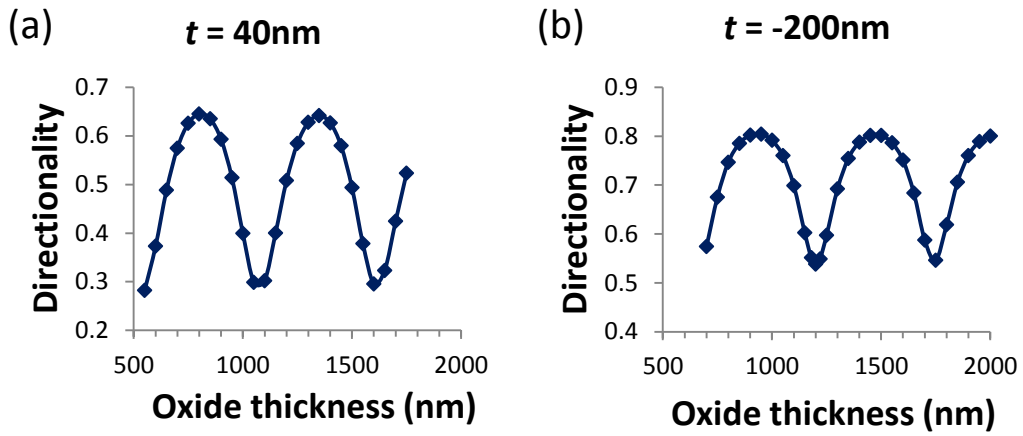

Fig. 2-5. The relations between directionality and thickness of oxide layer for grating height is (a) 40 nm and (b) -200 nm.

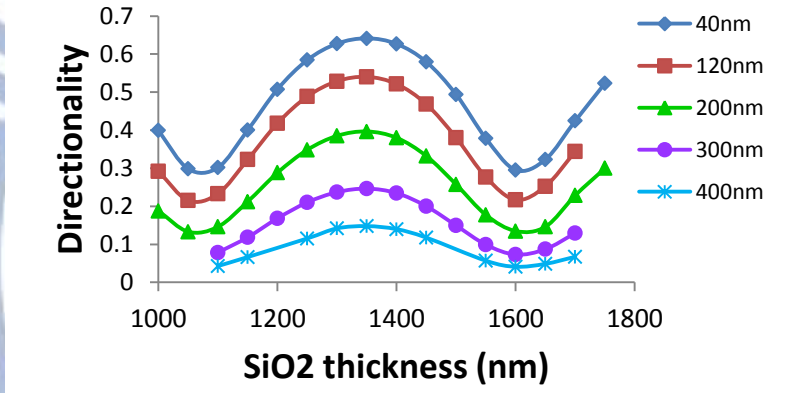

Fig. 2-6. The relations between directionality and thickness of oxide layer for upright grating with different grating height. Comparison of the directionality of upright grating using different grating height at varying oxide thickness.

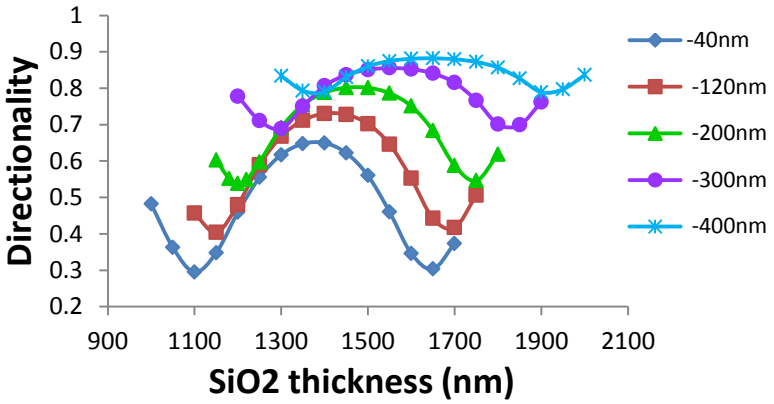

Fig. 2-7. The relations between directionality and thickness of oxide layer for buried grating with different grating height. Comparison of the directionality of buried

grating at varying oxide thickness.

We further compare the oscillation of directionality between several grating heights. Fig. 2-6 shows the result of upright grating. The directionality peaks of different heights coincide in the same oxide thickness. This is because both ray a and b go through the grating region. The increase in grating height doesn't change the difference of OPL, and only reduces the overall directionality by PBG effect. When grating height increases, the PBG effect becomes significant, and finally the directionality flattens and converges to 0 %.

However for buried grating, only the ray b goes through the grating region twice. The grating height changes the OPL with oxide thickness and therefore the peak directionality shifts correspondingly, as shown in Fig. 2-7 When grating height increases, PBG effect becomes significant, and finally the directionality saturates to 90 %.

Fig. 2-8 shows the field distributions when TE polarized light at 1550 nm is coupled into the waveguide and impinges gratings of t = -1000 nm, -200 nm, and 40 nm. Their FFs are all 30 %. For t = -1000 and -200 nm, the oxide thickness d is 1.45 μm. And for t = 40 nm, the oxide thickness d is 1.35 μm. It is obvious that wave propagating along waveguide is diffracted by the grating of t = -1000 nm without substrate loss. Almost all of the incident waves are diffracted upward. And therefore the directionality is 90 %. In the compromised case of t = -200 nm, there is substrate loss, but it is insignificant. The directionality of 80 % is still high. However in the upright case, it is obvious that the substrate loss is severe. And therefore the maximum directionality is only 64 %.

Because of the high refractive index contrast between metal stripes and surroundings, light can be diffracted out of the waveguide with grating of small stripe number. As shown in Fig. 2- 9, all -200 nm and -1000 nm buried grating, and 40 nm upright grating can attain their own highest directionalities when the gratings are composed of more than 20 stripes. And for grating of 20 stripes the total length is only about 12 μm. Again in the figure we can see that metal grating of buried design can attain higher directionality than that of the upright design.

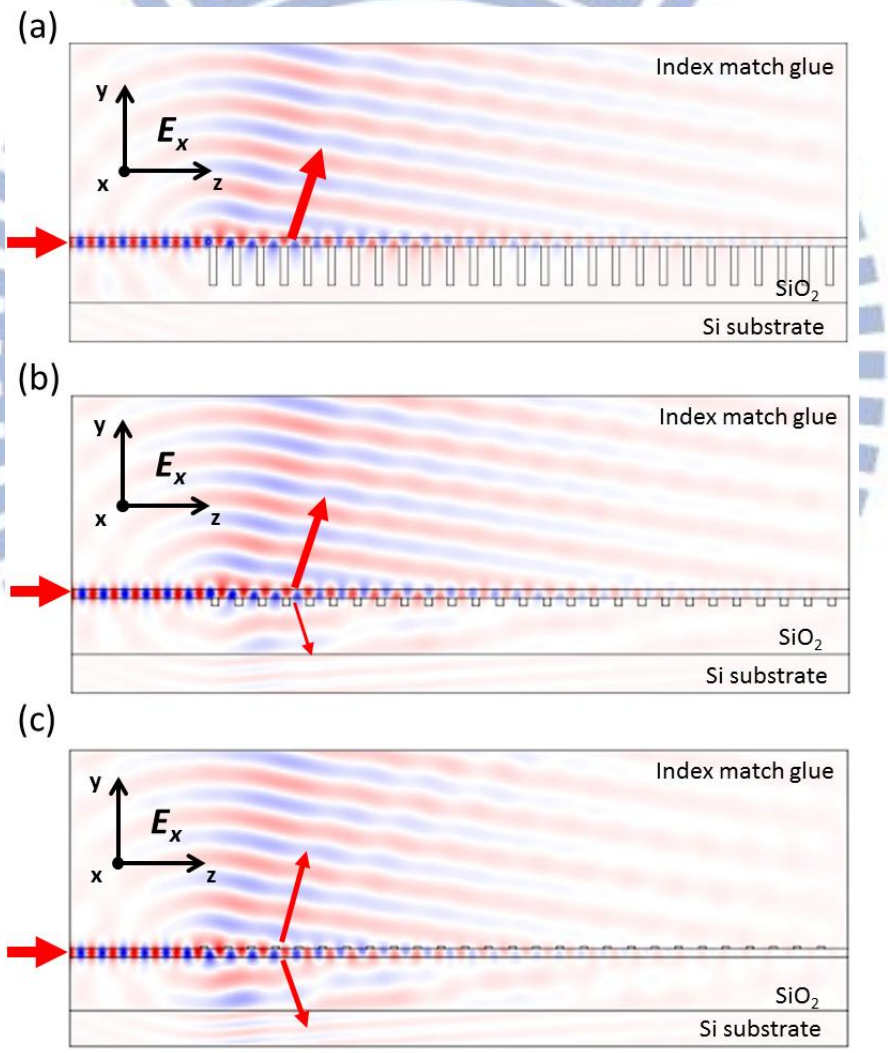

Fig. 2-8. Plots of x components of electric fields for the buried metal gratings of (a) $t = -1000$ nm and (b) $t = -200$ nm with 1.45μm oxide layer thickness. (c) Plots of x components of electric fields for the buried metal gratings of $t = 40$ nm with 1.35 μm oxide layer thickness.

strip number

Fig. 2- 9. The relations between directionality and number of the grating stripes under different grating height.

Finally we also compare our results with conventional silicon gratings. It had been reported that grating structure shallow-etched on silicon waveguide with apodization design (will be discussed in the next section) can reach 87.6 % directionality [10]. However very precise fabrication process is required to control each width of the grating grooves and get harmonic diffraction wave front as shown in Fig. 2-10 (a). If it is reduced to a uniform grating with 610 nm period and 40% FF, the directionality will decrease to 74.3% and the diffraction wave front will become complex as shown in Fig. 2- 10 (b).

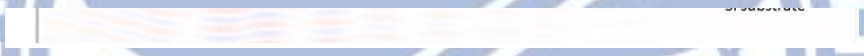

Fig. 2- 10. Plots of x components of electric fields for the silicon gratings (a) with apodization and (b) without apodization.

Fig. 2- 11. A plot of x component of electric fields for the silicon grating with wavelength of 1550 nm is in the band gap of the grating structure.

Even if we design the silicon grating with operation wavelength (1550 nm) in PBG, the effect does not prominent as shown in Fig. 2- 11. That is because both waveguide and grating are made by silicon. Waves impinging on the grating will partially bent into the stripes and become loss. As shown, the grating coupler cannot forbid waves propagating through the grating region, and thus the directionality is only 55.2%. Besides, the diffraction angle under these parameters is opposite to common designs. That will complicate the coupling scheme because input and output fibers may cross in the upper surrounding. So here we use gold as our grating material.

2-4-3 Dependence of directionality on grating filling factor

In the following discussion, we fix the oxide layer thickness at 1.45 μm, and investigate the dependences of directionality on *t* for FF ranging from 20 % to 60 %, as illustrated in Fig. 2-12. Operating wavelength at 1550 nm is within the photonic band gap of gratings for these FFs when period is 610 nm. It is obvious that, the directionality oscillates as a function of *t* for buried grating of small FF. The oscillation of directionality is caused by interference between rays a and b as above mentioned. However in the upright cases, directionality reduces monotonically as grating height increases no matter how large FF is. We can see that when FF increases from 20 % to 30 % the amplitude of oscillation reduces gradually. That means the interference between rays a and b in Fig. 2-3 (a) becomes weaker. That is because the operating wavelength will get closer to the center of PBG when the FF increases. And therefore the component of ray b is forbidden and reduces while most waves will be diffracted upward directly as ray a. The growing of overall direction supports this idea. When we further increase the FF from 20 % to 60 %, the oscillation of directionality becomes more and more flattened, however the value reduces progressively. This is because the inevitable metal absorption becomes severe when the FF increases. From the figure we can see that FF = 30 % for buried grating is most promising and can provide highest directionality not only for large but also for finite *t* values.

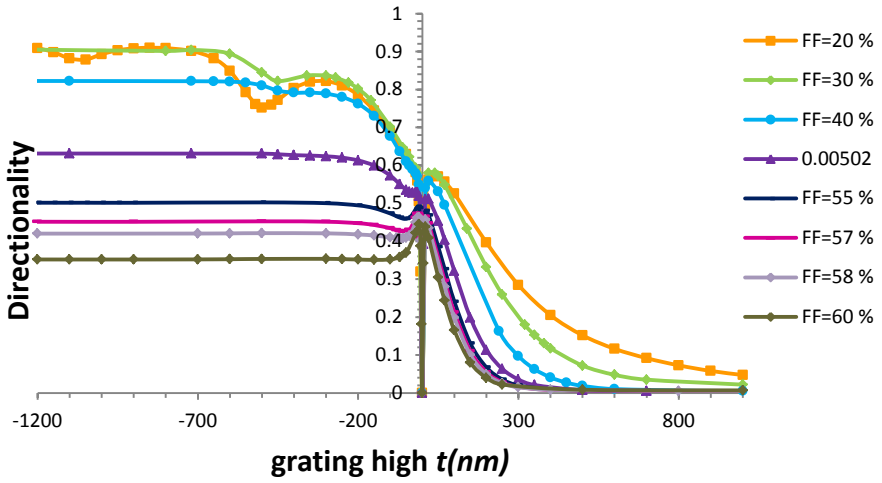

Fig. 2-12. The relations between directionality and grating height under different grating filling factor.

2-4-4 Apodization

From the above investigation we know a buried gold grating can achieve 90 % directionality when PBG effect is utilized and dominates over metal absorption. Besides, we also know that to improve the overall coupling efficiency of the grating, fiber mode overlap must be carefully considered. But for a uniform grating coupler, it is difficult to achieve high fiber mode overlap. This is because the diffracted wave declines exponentially along waveguide in z direction, but the mode of single mode fiber distributes as Gaussian function. These mode distributions are naturally out of match. So we use apodization design to make grating structure have Gaussian-shaped diffraction mode profile [10].

When waves propagating along the waveguide impinge the grating structure, some will be diffracted, and the remaining in the waveguide decay exponentially along the propagation direction as equation 2-8. describes.

$$P(z) = P_0 e^{-2\alpha z} \tag{2-8}$$

Where P*(*z*)* is the remaining power in the waveguide at z, P_0 is incident power of the waves before impinging the grating, and α is called the leakage factor or grating strength. And therefore the diffracted wave has an exponentially decaying power

$$P_{out} = \frac{\mathrm{d}P}{\mathrm{dz}} = -2\alpha P_0 e^{-2\alpha z} \tag{2-9}$$

along the propagation direction. For non-uniform grating structure, α becomes a function of z, and the diffracted mode profile can be shaped correspondingly. To achieve a Gaussian-shaped diffracted mode profile, $\alpha(\mathrm{z})$ is given by

$$2\alpha(z) = \frac{G^2(z)}{1-\int_0^z G^2(t)dt} \qquad (2\text{-}10)$$

where $G(z)$ is a normalized Gaussian profile. For coupling with standard single mode fiber at 1550 nm (diameter ratio of core/cladding is 8 μm/ 125 μm), we aim at generating a Gaussian distributed diffracted wave with 10.4 μm mode diameter. To achieve this z-dependent grating strength α, either grating height or filling factor can be varied [17, 24-26]. Considering the fabrication process, change filling factor is much either than change grating height. So we use changing filling factor to achieve Gaussian-shaped output beam. According to Eq. 2-9, we can get the grating strength by measuring the diffracted power of the grating. So we increase the grating filling factor from 0 to 0.9 and measurement the output power of each grating to get the relationship of FF and grating strength as shown in Fig. 2-13. And from Eq. 2-2, we know how to change the grating strength along the propagation direction z as shown in Fig. 2-14. We fix grating period and chose FF of each stripe of the grating to let grating strength vary in z direction as shown in Fig. 2-14.

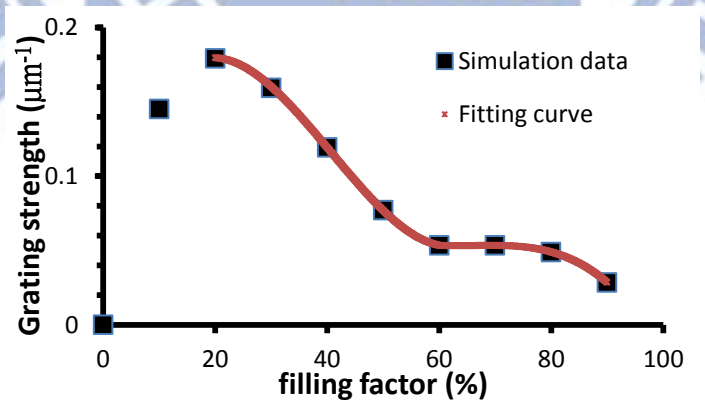

Fig. 2-13. The relations between grating strength and filling factor for buried grating with 200 nm grating height and its fitting curve.

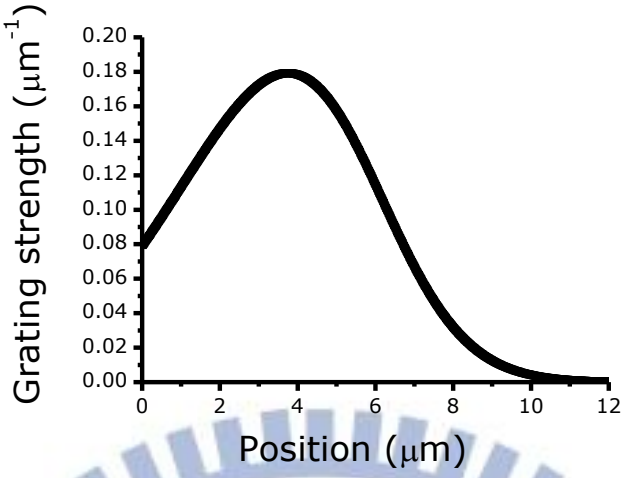

Fig. 2-14. The grating strength variation along the propagation direction z, which is for apodized grating has Gaussian-shaped output beam.

The apodized gratings were design for coupling between single-mode fibers with 10.4 μm mode field diameter and the fundamental TE mode in the waveguide. The coupling efficiency of 200 nm buried metal grating with uniform FF was 65 %. According to the dependence of grating strength on FF as shown in Fig. 2-13 we design the apodized grating with FFs listed in Table. 2-1. Finally we can attain the distribution of grating strength as shown in Fig. 2-14. The coupling efficiency of our apodized grating was 67.3%, which is better than uniform grating.

Stripe number	**1**	**2**	**3**	**4**	**5**	**6**	**7**	**8**	**9**	**10**
FF	**0.494**	**0.444**	**0.395**	**0.348**	**0.3**	**0.251**	**0.2**	**0.237**	**0.355**	**0.42**
Stripe number	**11**	**12**	**13**	**14**	**15**	**16**	**17**	**18**	**19**	**20**
FF	**0.237**	**0.237**	**0.237**	**0.237**	**0.237**	**0.237**	**0.237**	**0.237**	**0.237**	**0.237**

Table. 2-1. The filling factor of apodized grating designs with 20 stripes.

2-4-5 Alignment tolerance

The parameters of our grating structure have been analyzed in the previous section. But for a coupler, alignment tolerance is also an importance characteristic because it relates directly to reliability of a device. So we set a fiber as the input port, and lunch TE polarized fundamental fiber mode of 1550 nm wavelength with 1 W power. The mode is attained by using boundary mode analysis package in the software. Here we use apodized grating structure, with -200 nm height buried in 1.45 μm oxide layer, as the investigation target. The apodization rule of FF is as listed in table 2-1. First is the tolerance of coupling angle θ, which is the angle projected on yz-plane between the fiber axis and the direction perpendicular to the top surface of waveguide. As discussed before, the nonzero coupling angle is set to avoid back reflection at the grating. In this case, the optimal coupling angle is about 10.5°. A deviation on θ reduces the coupling efficiency, as shown in Fig. 2-15. An offset of 2° will reduce the overall coupling efficiency for about 16 % (1.19 dB additional loss).

Second is the influence of distance between the fiber facet and the grating as shown in Fig. 2-16 when fiber is aligned with optimal angle of 10.5°. Considering the diameter of the cladding layer, the minimum distance between fiber facet and the grating is about 12 μm as indicated in the inset. The coupling efficiency will reduce 12.5 % (0.8 dB additional loss) when the fiber moves from the optimal distance for 100 μm. And the nearer distance the fiber is, the higher the coupling efficiency is.

And then we investigate the tolerance of coupling position along z direction when fiber is aligned with optimal angle and is distant from the grating by 20 μm. The dependence of efficiency on the coupling position is shown in Fig. 2-17. The coupling

efficiency only reduces 5 % (0.32 dB additional loss) when the fiber moves from the optimal position for 1 μm.

Finally we investigate the tolerance of input wavelength when fiber is well aligned with optimal angle, distant and position. The bandwidth of 1 dB additional coupling loss is about 50 nm as shown in Fig. 2-15.

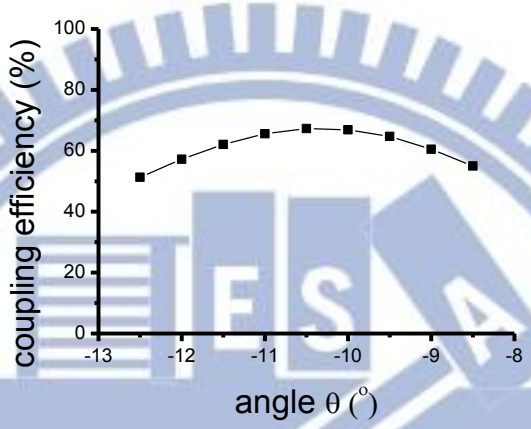

Fig. 2-15. The coupling efficiency as the function of the fiber angle.

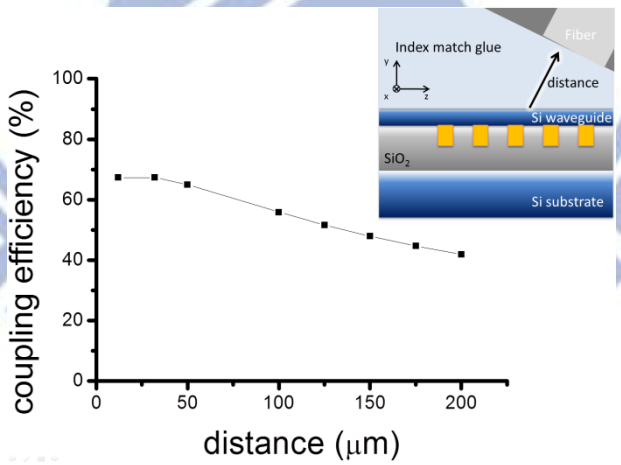

Fig. 2-16. The coupling efficiency as the function of the distance between fiber and waveguide.

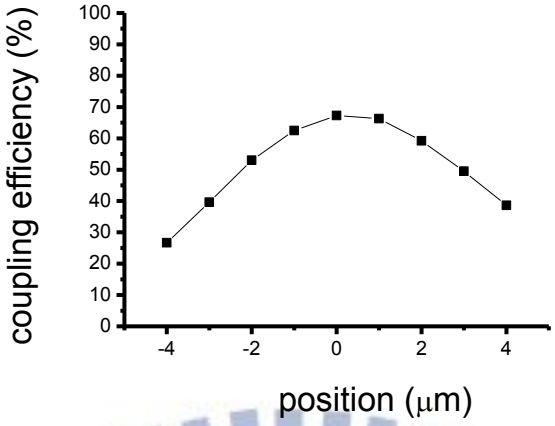

Fig. 2-17. The simulation results of the lateral alignment tolerances.

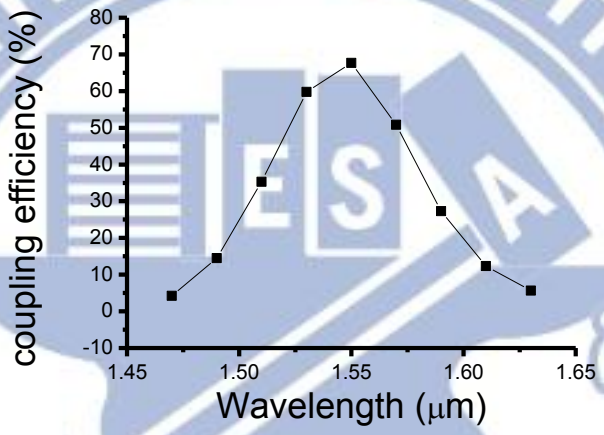

Fig. 2-15. The coupling efficiency as a function of input wavelength.

2-5 Summary

In this section, the gold grating structure with proper design can form PBG to forbid light propagating through it. The directionality therefore increases when grating buried under the waveguide eliminates substrate losses. The directionality finally saturate at 90% when the buried grating is higher than 1000 nm with FF = 30%. For adapting to practical fabrication, we choose -200 nm grating buried in 1.45 μm oxide layer. The 80% directionality is still high, and the overall coupling efficiency of 65% is higher than that reached by metal grating on top of waveguide. Considering fiber mode overlap, we also introduce apodization design to improve coupling efficiency up to 67.3%.

Chapter 3.

Fabrication and measurement

In this chapter we are going to present detail of fabrication processes and measurement results of the structure we design. The fabrication processes include making silicon waveguide, conductive assistant layer, and metal grating structure. And then we will show the system we setup for measuring and comparing the characteristics of upright and buried metal grating. Finally we will discuss the measured results in detail.

3-1. Fabrication

For fabricating the buried metal grating, an intuitive way is utilizing wafer bonding technique. One can first make grating structure on waveguide and deposit silicon oxide to cover all of the structures. Then bond the prepared sample to another substrate. Subsequently the original substrate can be removed by a series of physical and chemical etching. Finally the grating structure is transferred to be under the waveguide and the structure of buried metal grating is completed. However the whole process is quite complicated. And when it is completed we can only measure the directionality of the buried case. For comparing with the upright case, one will have to fabricate another upright metal grating on waveguide. But the upright and buried gratings must be attached to different waveguides made from different processes. There must be some uncontrollable inconsistence hindering fair comparison between the buried and upright cases. For experimental characterization, here we use quartz as our substrate in order to simplify the fabrication process because no bonding process

is required. Besides, it can solve the mentioned inconsistence. Due to the transparency of quartz substrate, we can collect both the diffractions from the top side and back side of the sample to evaluate directionalities of upright and buried grating, respectively, from the same waveguide.

Our waveguide structures are fabricated by etching poly silicon film on quartz substrate. The process flow is illustrated in Fig. 3-1. At first, we use sputter to deposit 200 nm amorphous-silicon film on the quartz substrate and anneal it at 1100 ℃ for three hours to get poly-crystallized film. Then a 1 μm AZ6112 photoresist layer is spun on the sample by spin coater. The strip pattern is defined on the photoresist layer by using photo-lithography with 10 μm width and 1 cm length. Then the pattern is transferred to poly-silicon layer by using reactive ion etching (RIE).

In the following processes metal grating structures will be fabricated on the waveguides by using electron beam lithography (EBL) and lift-off technique. However a shortage of using quartz substrate is its poor conductivity which will cause distortion of electron beam exposed images and patterns. Properly guiding the accumulated electrons will help solving these problems. Therefore we introduce aluminum mask layer surrounding the waveguides. They serve as neighboring metal tape used when taking images of scanning electron microscopic (SEM). The mask is defined by again photo lithography and followed by thermal evaporation of 130 nm aluminum. Then lift-off technique blanks out the region around the waveguides. This process flow is illustrated in Fig. 3-2. The nearest distance between aluminum mask edge and the waveguides is 10 μm.

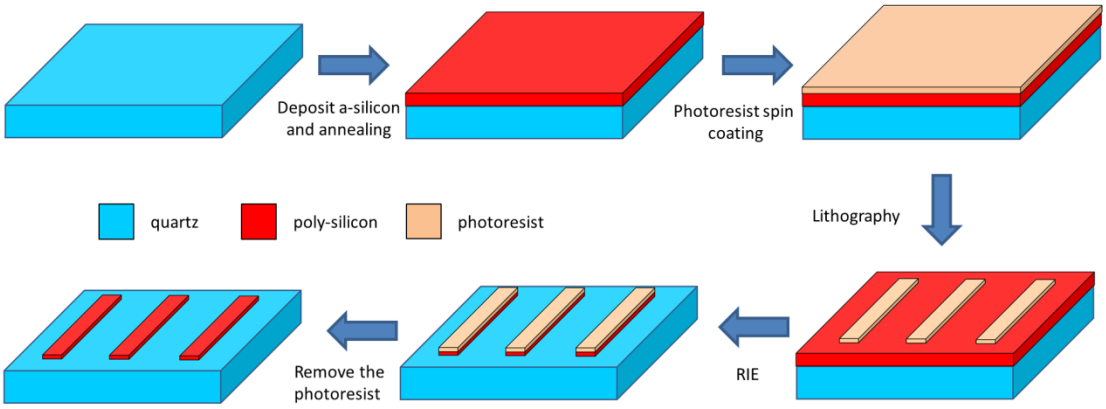

Fig. 3-1. The flow chart of the waveguide fabrication process.

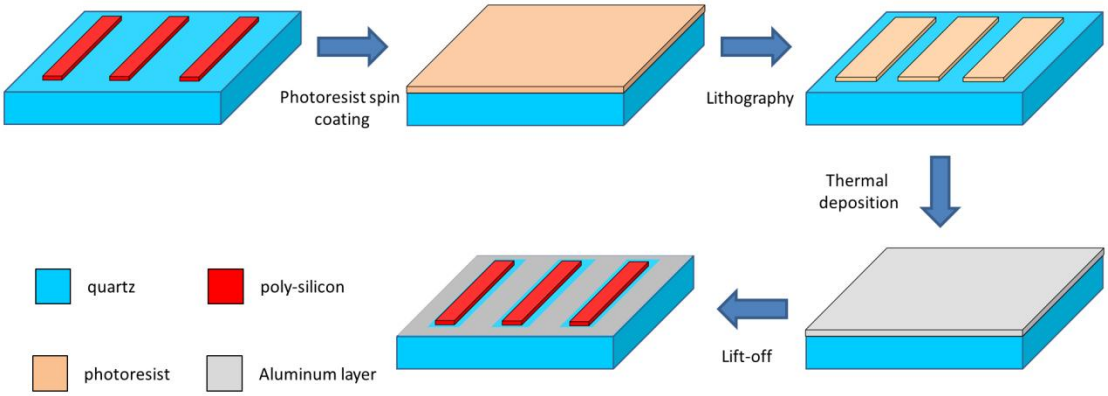

Fig. 3-2. The flow chart of the conductive layer fabrication process.

Then we fabricate grating structures on waveguides. The flow chart is shown in Fig. 3-3. First 240 nm polymethyl methacrylate (PMMA) layer is spun on the sample. The grating structures consisted by 30 periods of stripes with FF = 19 % and FF = 36 % are defined upon PMMA layer by using EBL. Because the grating structure must be right on the waveguides, alignment process must be implemented carefully. Then 120 nm gold is deposited again by thermal evaporator. And the pattern filled with gold is left on the waveguides by lift-off process. The SEM image of the grating structures are shown in Fig. 3-4. Because lift-off process is to tear off the gold film, the grating structure still has inevitable roughness.

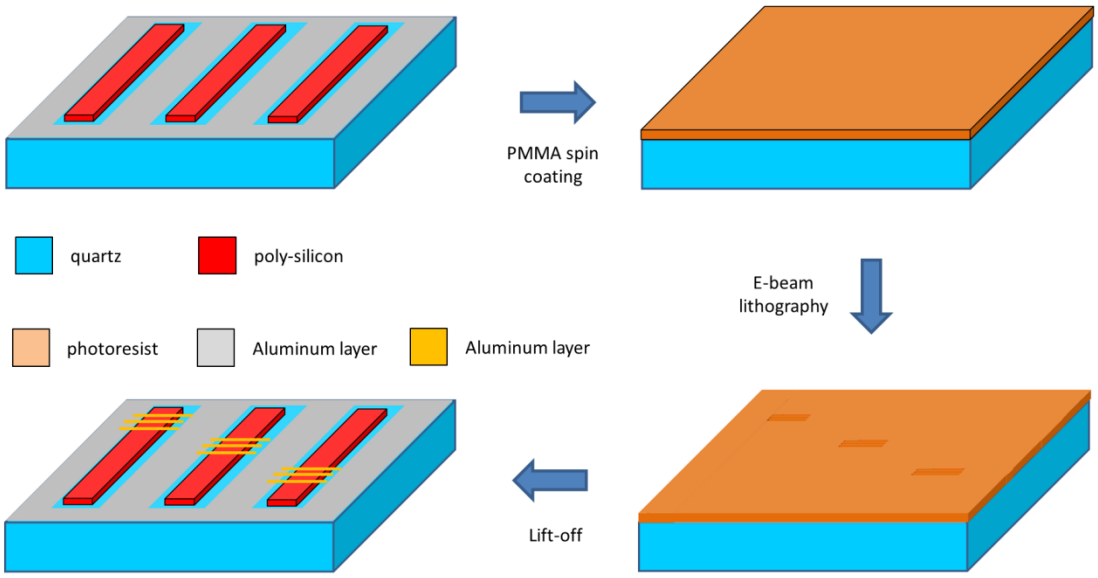

Fig. 3-3. The flow chart of the grating structure fabrication process. (BCB)

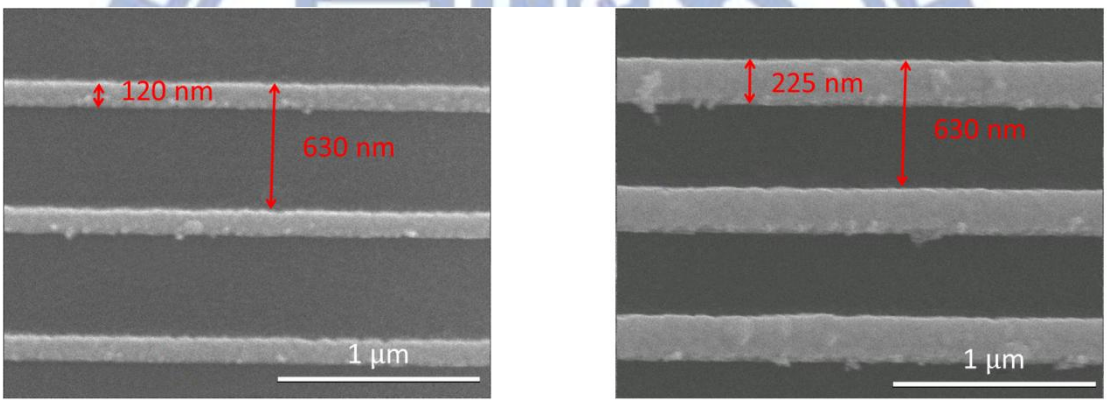

Fig. 3-4. The top-view SEM pictures of grating structures (a) FF = 19% (b) FF = 36%

Because in our measurement we will collect the diffractions from both top side and back side of the sample, we have to minimize the inconsistence between these two cases for fair comparison. However originally upward diffraction will propagate into free space directly, but downward diffraction will propagate into free space after transmit through quartz substrate. Therefore we cover an overlay with refractive index similar to quartz on top side of the sample to make index contrast above and below waveguide symmetric. Here the material of overlay we use is DVS-bis-Benzocyclobutene (commonly called BCB). After the grating structures are

completed, 4.4 μm BCB is spun on the sample. And then the sample is pre-cured at 60 ℃ for 4 minutes to eliminate bubbles inside. 250 ℃ hard-bake for 1 hour solidifies the BCB overlay.

In order to coupling light into the waveguides, we have to make entrances at one end of the waveguide for coupling. Generally, we used to cleave the substrate to complete this step, but quartz substrate is too hard to be cleaved precisely. So here we use process of mechanical grinding and polishing to make waveguide entrances expose for light coupling. During this process, surface of BCB would be attached with many grinded powders which will affect the following measurement negatively. So we cover whole sample with resin beforehand which also help the sample to be held stably during the process. The resin can be removed easily by dipped in acetone. Finally the all fabrication processes are completed and the sample is prepared for measuring.

3-2. Measurement setup

For characterizing the metal grating we couple light from tapered lens fiber into waveguide and collect both upward and downward diffracted power from grating to evaluate directionality of upright and buried cases, respectively. The measurement setup which we use to measure the diffracted power form grating is schematically illustrated in Fig. 3-5.

We clip one side of the sample with the clip side parallel to waveguides, and fix it to a pole which connects to a 3-Axes controllable stage as a sample stage. The continuous laser source is given by HP 8168 tunable laser (wavelength window ranging from 1480 nm to 1580 nm) and is amplified subsequently by an erbium

doped fiber amplifier. Output end of the amplifier is connected to a polarization rotator for controlling polarization state. Finally TE polarized laser transmits through a polarization maintaining fiber with tapered end for coupling. The fiber is mounted on a 6-axises adjustable micro-positioning stage and couples light into waveguides at the polished end of sample. We use continuous laser source at 1550 nm to do the following measurements. It is important to note that the sample stage and the 6-axises adjustable stage are on the same platform. So they can move simultaneously without relative displacement.

For collecting diffracted power from grating we build a system combining microscopic and power collecting utilities. In the optical axis of the system, a 100 x long working distance objective lens focuses illuminating white light at sample surface and collects all scattered light for observation. Except white light, the diffracted light from the grating will also be collected by the objective lens. The white light is mounted in the optical axis via a beam splitter (BS). After collimated by the objective lens and transmitting though the BS, the scattered white light is reflected by a mirror and focused again by a convex lens upon a charge-coupled device camera (CCD camera). Finally the image can be observed through a monitor. The mirror can be flipped. And when it is flipped, diffracted light collected from the sample will directly transmit, instead of being reflected, and be coupled into a multimode fiber (MMF) cable by another 2.5 x objective lens. Finally the output power is measured by Q8221 optical multi power meter. It is important that when measuring we will turn off all of the light sources (including ceiling lamp), only laser coupled into waveguide and diffracted from grating can be collected.

For measuring the upright gratings, the light collecting system focuses from the BCB side. We first use the microscopic utility to align the input end between fiber and waveguide. Here the white light is supplied from a secondary microscopic system in back of the sample as shown in Fig. 3-6, because image of fiber is clearer when white light illuminates from the back. The secondary microscopic system is mounted on the same platform with sample stage and fiber stage. Then we move the platform to make the system focus on grating for collecting diffracted power. Both diffraction collection and alignment of the input end will be optimized to get maximum output power.

For measuring the buried gratings, we turn the sample to let 100 x long working distance objective lens focus on the grating from quartz side. And we use the secondary microscopic system to align input side from the other side (BCB) with white light source from the collecting system. The secondary microscopic system is used because from the quartz side we cannot simultaneously focus on fiber and waveguide (the optical path length is different). Again the grating output is optimized both at the input end and the grating end by the collecting system.

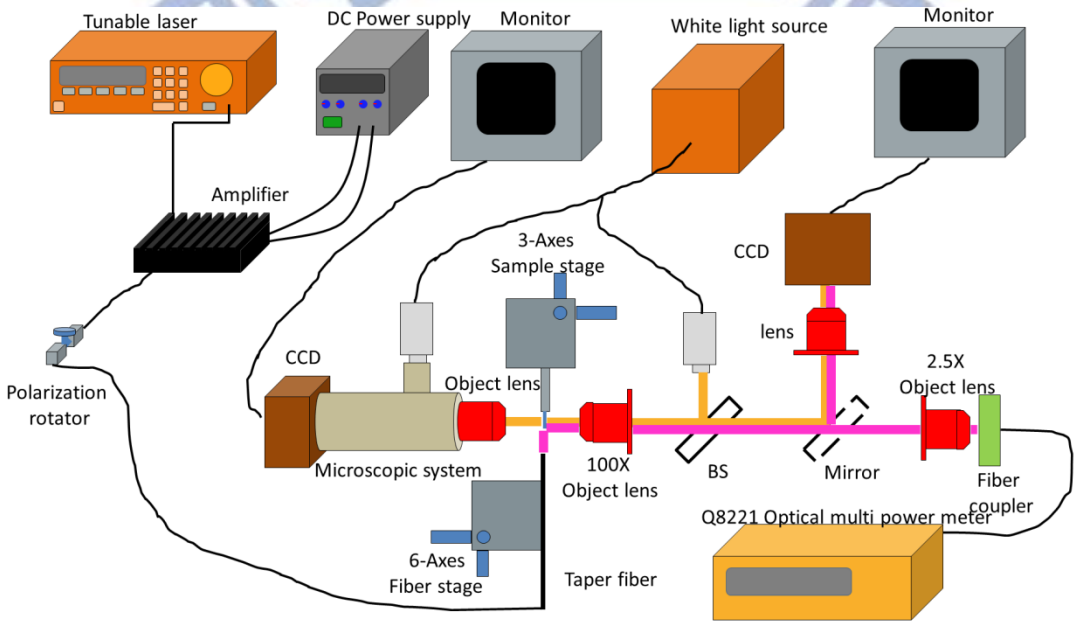

Fig. 3-5. Schematic of the measurement system.

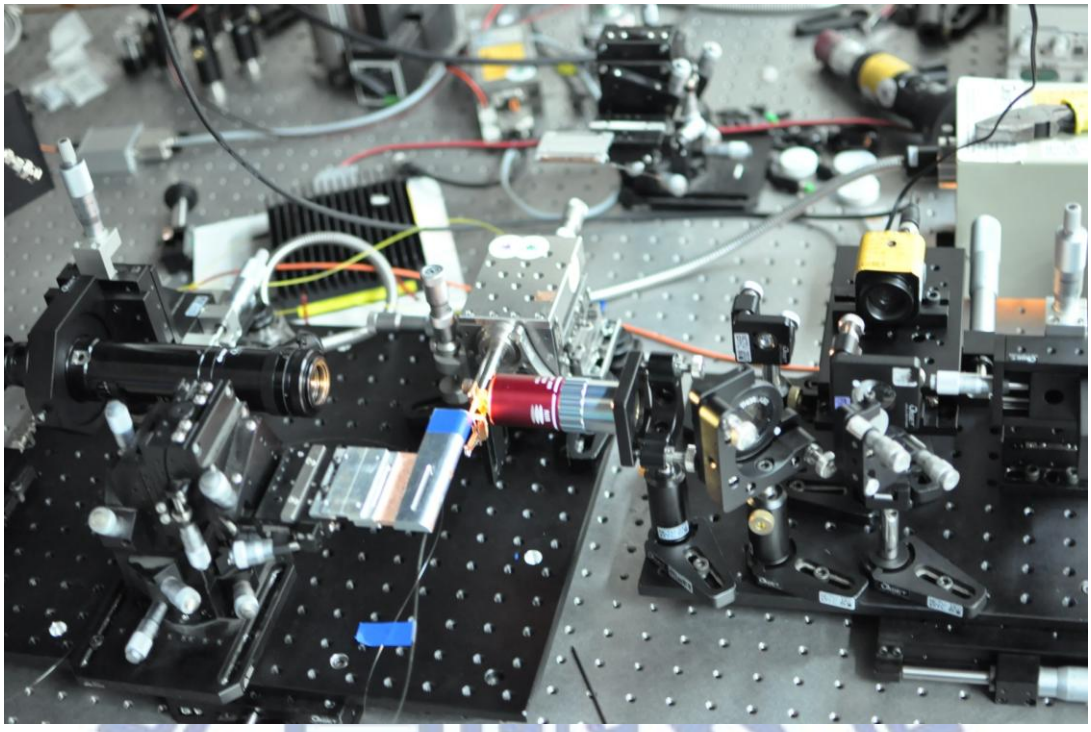

Fig. 3-6. The measurement setup for the upright grating. The white light is supplied from the back of sample.

3-3. Measurements and discussion

The grating couplers are fabricated at least 5 mm away from the input ports of the waveguide to avoid the waveguide to avoid collecting wave scattered directly from the input port. We measure fifteen measure fifteen waveguides at different distances from the input port on each waveguide (for each waveguide (for each distance there are three gratings on each waveguide and total is five different five different distances). Among three gratings with the same distance we find the results with the results with the highest diffracted power which is proportional to directionality of the grating. The grating. The results measured from grating with 19 % and 36 % FF are shown in Fig. 3-7 and Fig. 3-8, respectively. The FFs are measured by using SEM. It is obvious that for all distances the diffracted powers collected in the buried cases are much higher than those in the upright cases. Besides, gratings of 36 % FF perform better directionalities than those of 19 % FF gratings. That is because operating wavelength of 1550 nm is

closer to center of PBG for 36 % FF than for 19 % FF as we predicted in simulation works.

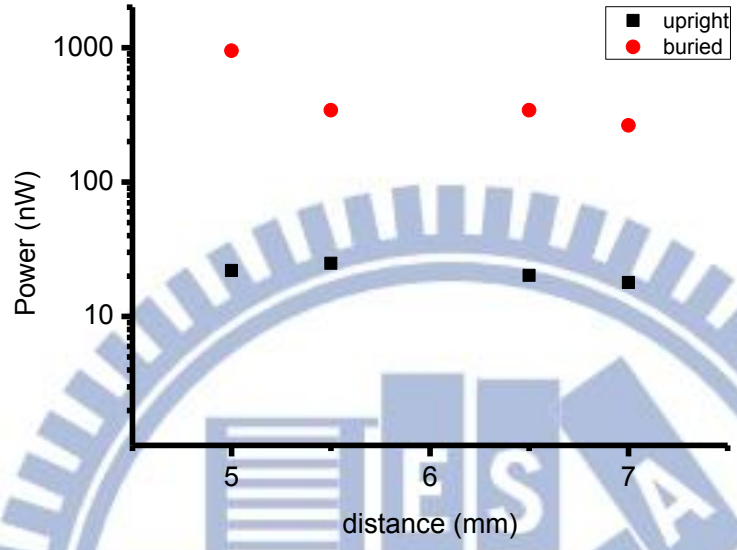

Fig. 3-7. The measurement output power from grating with FF=19% at different distance away from input port.

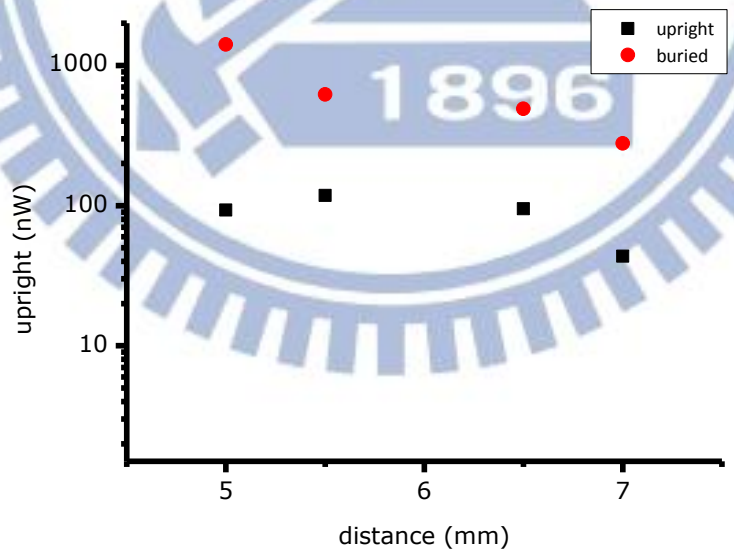

Fig. 3-8. The measurement output power from grating with FF=36% at different distance away from input port.

Because our grating structures are without the interface between oxide layer and silicon substrate, we simulate the directionality of different grating heights, in which the grating structures are without the interface for comparing with the experiment result. The results are shown in Fig. 3-9. Among the buried cases, grating with 30 % FF can reach the highest directionality for all grating height. In the range of small grating height, it is obvious that directionalities of gratings with 30, 35, and 40 % FF are higher than that with 20 % FF. So the result that directionality of grating with 36 % FF is higher than that with 19 % FF is reasonable. The only characteristic difference between gratings with and without the substrate interface is that there is no oscillation of directionality in the buried case because interference does not occur when there is no substrate interface. However the PBG effect caused by the grating itself still exists, so we can see that the directionality finally saturated as high as 90% when the buried grating is higher than 1000 nm. Finally we also directly observe the diffraction in the buried case by using infrared camera. As compared between Fig. 3-10 (a) and (b), the captured images clearly show the diffracted spot near the grating.

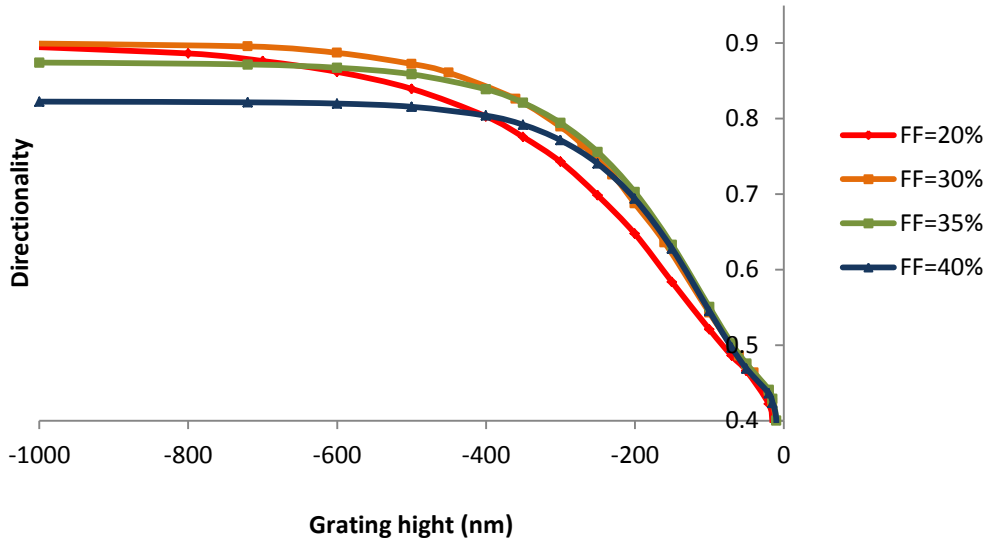

Fig. 3-9. The simulation result of grating high dependent of directionality with different FF.

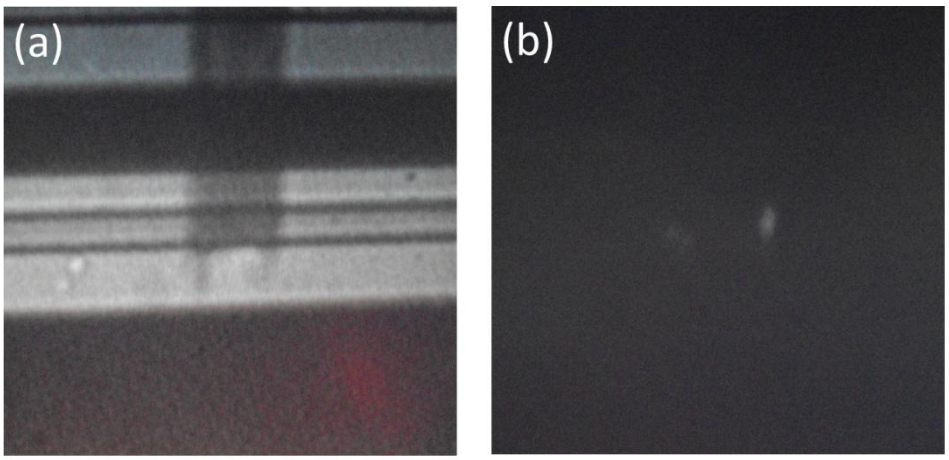

Fig. 3-10. The Image of the output power. (a) with back light, (b)without back light.

3-4. Summary

In this chapter, we present the fabrication processes of our grating structure. By introducing the aluminum mask layer, we solve the problem of charge accumulation which will make distortion of pattern exposed by electron beam lithography. The SEM picture shows that the pattern completed by our processes is quite good. From the measurement results, we can confirm that the buried grating couplers can reach higher directionality than that of the upright grating couplers. Even there is no substrate interface, the PBG effect still dominates and makes the directionality of diffraction high.

Chapter 4.

Conclusion and Future work

4-1 Conclusion

In this research, we attempt to design an efficient fiber-waveguide coupler without the need of wafer-cleaving. Grating structure can serve as coupler between fiber and waveguide with vertical arrangement. In this configuration waves propagating along waveguide can be diffracted out of the plane of waveguide and coupled into a neighboring fiber which is nearly perpendicular to the plane. Due to the reversibility of optical path the wave can also be coupled from the perpendicular fiber into the waveguide. However for most designs the diffraction has equal components propagating upward and downward respectively. But only the upward diffraction toward fiber is available. So the directionality of grating coupler is always limited at 50 %. For overcoming this limitation we incorporate PBG effect into the grating coupler. We chose gold as the material of our grating structure because metal grating can be fabricate simply by lift-off technique which saves the fabrication process. Besides, we have found that the grating structure can be regarded as a 1-D photonic crystal with PBG which will forbid light transmitting through the grating region. The operating wavelength of 1550 nm is just within the PBG of gold grating when grating parameters are chosen for diffraction of single order. We use this characteristic to design a buried gold grating coupler. By burying the gold grating under waveguide, we can eliminate diffraction toward substrate and improve the directionality of diffraction toward fiber. We use FEM simulation to investigate wave at 1550 nm propagating along silicon waveguide and being diffracted by the grating. Simulation

results show that buried grating does have better directionality than the upright counterpart. When height of the buried grating is larger than 1000 nm, the directionality saturates as high as 90% because the gold grating forms complete PBG and forbids waves transmitting downward. In this case most waves will be diffracted upward toward the fiber. For adapting to practical situation, we choose 200 nm grating buried in 1.45μm oxide layer as target. The 80% directionality is still very high.

Considering fiber mode overlap, we introduce apodization design to make diffraction of the grating have Gaussian profile. The coupling efficiency of grating with apodization is 67.3%. However in reference utilizing upright metal grating the maximum coupling efficiency is only 50 % [20]. Our result attributes to high directionality of the buried structure and the apodization design. When we move the fiber position in z (longitudinal) direction for 1 μm away from the optimize position, the coupling efficiency only reduces 5%. And the coupling efficiency reduces about 10% when fiber is moved 100 μm away from the grating in y (vertical) direction. In experiment, our grating structure is fabricated by e-beam lithography and lift-off technique. For overcoming the distortion caused by charge accumulation, we add conductive mask layer before writing the grating pattern by EBL. Therefore fine grating stripes can be attained. In measurement, the results show that buried grating couplers have better directionality than upright grating as predicted by simulation.

4-2 Future work

4-2-1 Adjusting lateral mode size by tuning waveguide width

In chapter 2-4, we had done complete 2-D simulation. But a 3-D simulation will be more convincing because in 2-D simulation we only consider the diffraction phenomenon in longitudinal and vertical directions. For understanding the real situation we need 3-D FEM to do simulation. But a precise 3-D numerical analysis will need numerous elements to do the calculation in COMSOL software. Our computational system does not afford because that will occupy more than 64 G ram (upper bound of our system). So here we just perform characteristic analysis of the target structure. The structure parameters used in simulation are listed in Table. 4-1.

	Diameter
a	610 nm
t	-200 nm
d	1.45 μm
FF	30%
Waveguide thickness	220 nm
Waveguide width (*l*)	2-10 μm

Table. 4-1. Simulation parameters of waveguide and grating structure.

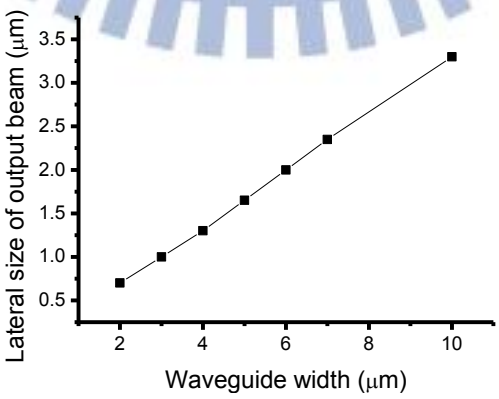

Fig. 4-1. The *l* dependences of lateral mode size.

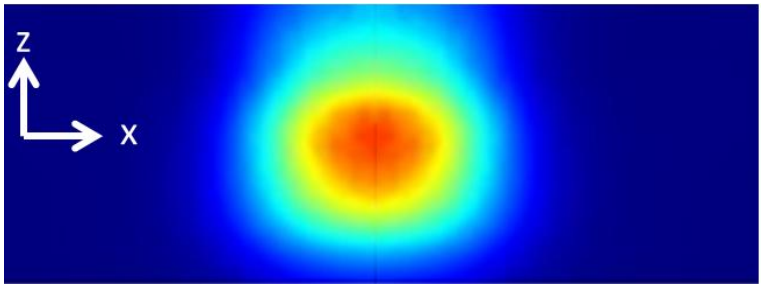

Fig. 4-2. The output power profile in xz plane with waveguide width at 3μm.

As shown in Fig. 4-1, the size of output beam in x direction increases linearly as a function of waveguide width (*l*). But the mode size in z direction fix at 0.9 μm independent of *l*. By reducing *l* to 3 μm we can get a nearly circular output beam (~ 0.9 μm mode diameter) as shown in Fig. 4-2. That is advantageous because circular output beam will have higher coupling efficiency with circular fiber mode than elliptical output beam. If apodization technique is incorporated with corresponding waveguide width we believe a circular diffraction mode well matching fiber mode can be generated and further enhance the coupling efficiency. In the future we will do more detail analysis after we improve our computer system.

4-2-2 Improvement of experimental demonstration

To demonstrate utility of the buried grating coupler, a measurement approach following how the coupler works will be more convincing. That is, we should probe waveguide with buried gratings as input and output ports by two optical fibers at these ports respectively. Light will be coupled from first fiber into waveguide through a buried grating and be collected by second fiber at output port of another buried grating. With this scheme we can get the entire efficiency of the system. By investigating the influence caused by reducing the distance between these two gratings, we can also obtain propagation loss of the waveguide. Then the whole system is analyzed. These measurements will be done in our following works.

4-2-3 Further application in passive component

To date, passive devices with various new functionalities have been proposed. In our research scope, plasmonic structures and photonic crystal structures are designed to serve sensing, molecule detection, or optical manipulation. However for the purpose of chip integration, exciting devices by coupling light from neighboring waveguide would be more promising. So at the same time when we design integrated devices, we have to build up a coupling system for input and output of light. Now buried grating coupler is the candidate. In the following works we will devote to integrating the grating coupler with our devices, to bring a complete system prototype.

Reference

[1] W. Bogaerts, R. Baets, P. Dumon, V. Wiaux, S. Beckx, D. Taillaert, B. Luyssaert, J. Van Campenhout, P. Bienstman, and D. Van Thourhout, "Nanophotonic waveguides in silicon-on-insulator fabricated with CMOS technology," *Journal of Lightwave Technology,* vol. 23, pp. 401-412, Jan 2005.

[2] T. Shoji, T. Tsuchizawa, T. Watanabe, K. Yamada, and H. Morita, "Low loss mode size converter from 0.3 mu m square Si wire waveguides to singlemode fibres," *Electronics Letters,* vol. 38, pp. 1669-1670, Dec 5 2002.

[3] S. J. McNab, N. Moll, and Y. A. Vlasov, "Ultra-low loss photonic integrated circuit with membrane-type photonic crystal waveguides," *OPTICS EXPRESS,* vol. 11, pp. 2927-2939, Nov 3 2003.

[4] A. Khilo, M. A. Popovic, M. Araghchini, and F. X. Kartner, "Efficient planar fiber-to-chip coupler based on two-stage adiabatic evolution," *OPTICS EXPRESS,* vol. 18, pp. 15790-15806, Jul 19 2010.

[5] M. Fritze, J. Knecht, C. Bozler, C. Keast, J. Fijol, S. Jacobson, P. Keating, J. LeBlanc, E. Fike, B. Kessler, M. Frish, and C. Manolatou, "Fabrication of three-dimensional mode converters for silicon-based integrated optics," *Journal of Vacuum Science & Technology B,* vol. 21, pp. 2897-2902, Nov-Dec 2003.

[6] M. C. M. Lee, W. C. Chiu, T. M. Yang, and C. H. Chen, "Monolithically integrated low-loss silicon photonic wires and three-dimensional tapered couplers fabricated by self-profile transformation," *Applied Physics Letters,* vol. 91, Nov 5 2007.

[7] N. Fang, Z. F. Yang, A. M. Wu, J. Chen, M. Zhang, S. C. Zou, and X. Wang, "Three-Dimensional Tapered Spot-Size Converter Based on (111) Silicon-on-Insulator," *Ieee Photonics Technology Letters,* vol. 21, pp. 820-822, May-Jun 2009.

[8] C. W. Liao, Y. T. Yang, S. W. Huang, and M. C. M. Lee, "Fiber-Core-Matched Three-Dimensional Adiabatic Tapered Couplers for Integrated Photonic Devices," *Journal of Lightwave Technology,* vol. 29, pp. 770-774, Mar 1 2011.

[9] M. Antelius, K. B. Gylfason, and H. Sohlstrom, "An apodized SOI waveguide-to-fiber surface grating coupler for single lithography silicon photonics," *OPTICS EXPRESS,* vol. 19, pp. 3592-3598, Feb 14 2011.

[10] X. Chen, C. Li, C. K. Y. Fung, S. M. G. Lo, and H. K. Tsang, "Apodized Waveguide Grating Couplers for Efficient Coupling to Optical Fibers," *Ieee*

Photonics Technology Letters, vol. 22, pp. 1156-1158, Aug 1 2010.

[11] M. K. Emsley, O. Dosunmu, and M. S. Unlu, "Silicon substrates with buried distributed Bragg reflectors for resonant cavity-enhanced optoelectronics," *Ieee Journal of Selected Topics in Quantum Electronics,* vol. 8, pp. 948-955, Jul-Aug 2002.

[12] F. Van Laere, G. Roelkens, J. Schrauwen, D. Taillaert, P. Dumon, W. Bogaerts, D. Van Thourhout, and R. Baets, "Compact grating couplers between optical fibers and Silicon-on-Insulator photonic wire waveguides with 69% coupling efficiency," *2006 Optical Fiber Communication Conference/National Fiber Optic Engineers Conference, Vols 1-6,* pp. 2684-2686, 2006.

[13] G. Roelkens, D. Van Thourhout, and R. Baets, "High efficiency Silicon-on-Insulator grating coupler based on a poly-Silicon overlay," *OPTICS EXPRESS,* vol. 14, pp. 11622-11630, Nov 27 2006.

[14] F. Van Laere, G. Roelkens, M. Ayre, J. Schrauwen, D. Taillaert, D. Van Thourhout, T. E. Krauss, and R. Baets, "Compact and highly efficient grating couplers between optical fiber and nanophotonic waveguides," *Journal of Lightwave Technology,* vol. 25, pp. 151-156, Jan 2007.

[15] S. K. Selvaraja, D. Vermeulen, M. Schaekers, E. Sleeckx, W. Bogaerts, G. Roelkens, P. Dumon, D. Van Thourhout, and R. Baets, "Highly efficient grating coupler between optical fiber and silicon photonic circuit," *2009 Conference on Lasers and Electro-Optics and Quantum Electronics and Laser Science Conference (Cleo/Qels 2009), Vols 1-5,* pp. 1293-1294, 2009.

[16] G. Roelkens, D. Vermeulen, S. Selvaraja, R. Halir, W. Bogaerts, and D. Van Thourhout, "Grating-Based Optical Fiber Interfaces for Silicon-on-Insulator Photonic Integrated Circuits," *Ieee Journal of Selected Topics in Quantum Electronics,* vol. 17, pp. 571-580, May-Jun 2011.

[17] D. Taillaert, F. Van Laere, M. Ayre, W. Bogaerts, D. Van Thourhout, P. Bienstman, and R. Baets, "Grating couplers for coupling between optical fibers and nanophotonic waveguides," *Japanese Journal of Applied Physics Part 1-Regular Papers Brief Communications & Review Papers,* vol. 45, pp. 6071-6077, Aug 2006.

[18] G. Roelkens, D. Vermeulen, D. Van Thourhout, R. Baets, S. Brision, P. Lyan, P. Gautier, and J. M. Fedeli, "High efficiency diffractive grating couplers for interfacing a single mode optical fiber with a nanophotonic silicon-on-insulator waveguide circuit," *Applied Physics Letters,* vol. 92, Mar 31 2008.

[19] R. Orobtchouk, A. Layadi, H. Gualous, D. Pascal, A. Koster, and S. Laval, "High-efficiency light coupling in a submicrometric silicon-on-insulator

waveguide," *Applied Optics,* vol. 39, pp. 5773-5777, Nov 1 2000.

[20] S. Scheerlinck, J. Schrauwen, F. Van Laere, D. Taillaert, D. Van Thourhout, and R. Baets, "Efficient, broadband and compact metal grating couplers for silicon-on-insulator waveguides," *OPTICS EXPRESS,* vol. 15, pp. 9625-9630, Jul 23 2007.

[21] E. Yablonovitch, "Inhibited Spontaneous Emission in Solid-State Physics and Electronics," *Physical Review Letters,* vol. 58, pp. 2059-2062, May 18 1987.

[22] S. John, "Strong Localization of Photons in Certain Disordered Dielectric Superlattices," *Physical Review Letters,* vol. 58, pp. 2486-2489, Jun 8 1987.

[23] J. Jin, *The Finite Element Method in Electromagnetics*, 2 ed. Wiley,New York, 2002.

[24] A. Mekis, S. Gloeckner, G. Masini, A. Narasimha, T. Pinguet, S. Sahni, and P. De Dobbelaere, "A Grating-Coupler-Enabled CMOS Photonics Platform," *Ieee Journal of Selected Topics in Quantum Electronics,* vol. 17, pp. 597-608, May-Jun 2011.

[25] D. Taillaert, P. Bienstman, and R. Baets, "Compact efficient broadband grating coupler for silicon-on-insulator waveguides," *Optics Letters,* vol. 29, pp. 2749-2751, Dec 1 2004.

[26] K. A. Bates, L. F. Li, R. L. Roncone, and J. J. Burke, "Gaussian Beams from Variable Groove Depth Grating Couplers in Planar Wave-Guides," *Applied Optics,* vol. 32, pp. 2112-2116, Apr 20 1993.